INVESTIGATION OF PAIR DISTRIBUTION FUNCTION METHOD ON STRUCTURAL ANALYSIS OF X-RAY DIFFRACTION DATA FROM NANOCRYSTALLINE POWDERS

A Thesis

by

Abolfazl Baloochiyan

Submitted to the

Graduate School of Sciences and Engineering
In Partial Fulfillment of the Requirements for
the Degree of

Master of Science

in the
Department of Mechanical Engineering

Özyeğin University
December 2021

INVESTIGATION OF PAIR DISTRIBUTION FUNCTION METHOD ON STRUCTURAL ANALYSIS OF X-RAY DIFFRACTION DATA FROM NANOCRYSTALLINE POWDERS

Approved by:

Dr. Hande Öztürk Kaymaksüt, Advisor,
Department of Mechanical Engineering
Özyeğin University

Dr. İlknur Eruçar Fındıkçı,
Department of Natural and Mathematical Sciences
Özyeğin University

Dr. Erkan Şenses,
Department of Chemical and Biological Engineering
Koç University

Date Approved: December 2021

ABSTRACT

Pair Distribution Function analysis is a local characterization method gaining momentum recently. Conventional X-ray diffraction and Rietveld methods have proven not to be accurate in the case of analysis of diffraction data from nanocrystalline powders [1]. In this thesis, we evaluate the accuracy of this alternative technique, which is based on a refinement algorithm in real space, and because of being in real space, the properties obtained from this method are more intuitive. Structural parameters like particle size, neighbor atomic distances, etc. are obtained by directly calculating the distances and area of each peak or distance.

Large surface to volume atom ratio is stated to be the reason that makes it hard for conventional X-ray diffractive methods to characterize nanocrystals. Because conventional methods have a fundamental assumption about the materials and that is large crystalline domains in the scattering material. Unfortunately, nanocrystalline powders do not satisfy this assumption. Surface atoms, because of lack of neighbor atoms around them, have a small coordination number, as a result, they do not fulfill crystallinity. However, Pair Distribution Function can obtain the structure of the materials, regardless of their crystallinity. It is claimed that amorphous materials can also be analyzed in this method [2]. The probability of finding two atoms at a special distance from each other, is the basic point of view. This method is being used in different areas of study including drug delivery [3], materials characterization [4], fracture mechanics [5], [6], condensed matter physics [7], etc. and recently it has been

gaining momentum, especially where the conventional diffractive characterization methods cannot have an exact answer for structural properties.

Although being a fairly developed algorithm, Pair Distribution Method still needs work to become perfect. For instance, the strain of the particles still cannot be calculated directly in this method, and Diffpy-Complex Modeling Infrastructure is intricate for the ones who are not familiar with object-oriented programming. In this research, we are looking at different approaches towards obtaining the necessary parameters from Pair Distribution Function fitting, goodness of the fits, and validity of the results.

The systematic analysis of our work consists of five different nanocrystalline sizes and five different wavelengths, for both ideal nanocrystalline materials and energy minimized nanocrystals in 0 K temperature. The results of Pair Distribution Function show as the nanocrystalline size decreases the amount of crystallinity for the energy-minimized nanocrystals decrease. As the nanocrystals decrease in their size, the obtained values of lattice parameter decrease in comparison with the nominal lattice parameters. Atomic Displacement Parameters for the energy-minimized nanocrystals show a higher value for the smallest nanocrystalline sizes. Also, the predicted nanocrystalline size from this method gives slightly smaller size values which are attributed to the prediction of the peak attenuation. The lowest wavelength X-ray has the highest energy. For the highest energy wavelength, the Pair Distribution Function fit results of the particle size shows the size of the minimized particles is slightly less than the size of the ideal counterparts.

ACKNOWLEDGMENTS

First of all, I would like to thank my advisor Dr. Hande Öztürk Kaymaksüt, for her outstanding support in every aspect of my graduate studies. She is one of the most severe and professional academicians I have ever seen. She is extraordinarily time efficient. Her endorsement for the students is exemplary, and words cannot express my gratitude for her relentless care about me. Having Dr. Öztürk as my advisor was, and will be, one of my most excellent academic experiences, and I am forever indebted to her.

Secondly, I would appreciate all the guidances of my other instructors, Dr. İlknur Eruçar Fındıkçı for being a very kind instructor, and Dr. Kadir Durak for letting me know about the incredible capabilities of physics and the precious points of view about life and academia.

Thirdly, I appreciate my groupmates, Merdan Batyrov and Hamidreza Hekmatjou, for being sincere and hard-working friends who always inspired me to work better. Without their help, my thesis could never finish. I used Merdan's results in large. His significant experience in coding, especially with R, is fascinating. We had countless hours of debate about his codes. I also appreciate my other instructors who have always supported me and answered all my questions, although having a full schedule; Dr. Polat Şendur, Dr. Altuğ Başol, and Dr. Zeynep Başaran Bundur.

Lastly, my family suffered a lot to let me follow my dreams. I am speechless when it comes to talking about my family. They are dealing with millions of hardships to help me with my future ambitions. I only can wish them health and happiness.

This project was done under TUBITAK 2232 International Fellowship of Outstanding Researchers (Project No: 118C238).

TABLE OF CONTENTS

LIST OF TABLES

LIST OF FIGURES

NOMENCLATURE

ABBREVIATION	DEFINITION
3D	3 dimensional
Å	Angstrom
a, b, c	Lattice parameters
α, β, γ	Lattice angles
ADP	Atomic displacement parameter
BCC	Body centered cubic
CIF	Crystallographic Information File
CN	Coordination number
DSE	Debye Scattering Equation
f	Atomic scattering factor
F(Q)	Reciprocal space scattering
FCC	Face centered cubic
FWHM	Full width at half maximum
I	Intensity of the peaks
K	Scherrer constant
λ	X-ray wavelength
MD	Molecular dynamics
nm	Nanometer
PDF	Pair distribution function
θ	Half the scattering angle
Q	Momentum transfer matrix
Q_{damp}	Damping factor
Q_{max}	Maximum momentum transfer vector
Q_{min}	Minimum momentum transfer vector
r_{ij}	distance vector
RMS	Root mean square
Rw	Residual weighted
S(Q)	Structure factor
SC	Simple cubic
STV	Surface to volume
x_0	Lorentzian peak center
μ	Mean of Gaussian distribution
$\rho(r)$	Real space pair density
ρ_0	Number density
σ	Standard deviation of Gaussian distribution
ω	periodicity of the Fourier transfer
Γ	Lorentzian peak width
B	Breadth of the peak

CHAPTER I

INTRODUCTION

Wilhelm Conrad Röntgen discovered X-rays in 1895 [8]. They are vastly used in different branches of science, including the physics of materials and medical sciences [9], [10]. X-ray Scattering and diffraction thrived in the early 1900 by Max Theodor Felix von Laue and Sir William Henry Bragg who won Noble prizes for their efforts on X-ray diffraction and crystallography in 1914 and 1915, respectively [11], [12]. Bragg found an equation which relates the wavelength of X-ray to the interatomic plane distances in a crystal [12], [13]. This relation can be named as the fundamental equation of X-ray and crystallography [14], [15]:

$$2\,d \sin\theta = n\,\lambda \qquad (1)$$

λ is the wavelength of the X-ray, θ is half the scattering angle, and d is the interplanar distance of the crystal structure. Eq. (1) gives the position of constructive interference in the "Intensity vs. 2θ" graph. Bragg's law relates interplanar distances to the reflection angles. Intensity of the peaks is obtained experimentally, by diffractometers. However, we used simulated X-ray diffraction patterns mainly because our focus is to understand the impact of different conditions on the PDF and diffraction pattern of powder nanocrystalline structures and observe its effect on the properties of the samples. For simulations, an analytical X-ray diffraction equation proposed by the German physicist,

Peter Joseph William Debye is used. This equation yields noiseless diffraction patterns for powder nanocrystals. As mentioned, a noiseless diffraction pattern is essential to learn the diffraction and PDF, related properties, and determining factors.

Debye published the article "Zerstreuung von Röntgenstrahlen" meaning scattering of X-rays in 1915 [16]. In this article, he revealed his equation, nowadays known as Debye Scattering Equation (DSE) [17]–[19]:

$$I_{avg}^{Debye}(\vec{Q}) = f_m(\vec{Q})\, f_n(\vec{Q}) \sum_{i=1}^{N}\sum_{j=1}^{N} \frac{\sin\left(|\vec{Q}|\,|\vec{r}_{ij}|\right)}{|\vec{Q}|\,|\vec{r}_{ij}|} \qquad (2)$$

N stands for the total number of atoms in the particle, f is the atomic scattering factor, $|\vec{Q}|$ is the magnitude of the momentum transfer vector and is equal to $\frac{4\pi \sin\theta}{\lambda}$. The distance vector between each pair of atoms is defined as $\vec{r}_{ij} = \vec{r}_i - \vec{r}_j$, where the origin is an arbitrary point in the particle volume. In order to obtain the intensities out of Debye Scattering Equation (DSE), one should loop two times over the atoms, the first loop will determine i^{th} atom and the second loop will loop over j^{th} atom. $|\vec{Q}|$ is a function of θ, as a result, for each θ there is a double summation over all atoms in the particle. There are some methods to reduce the computation time, for instance, in order to calculate the atomic distances, one can only calculate $\vec{r}_{ij}$ once and save it in order not to recalculate for every angle. In a non-optimized manner, $\vec{r}_{ij}$ is calculated two times because it also includes $\vec{r}_{ij}$. When not optimized, evaluation of DSE for a 5 nm gold

nanocrystal which has 3589 atoms, takes almost 7,000 seconds in MATLAB on a standard laptop computer.

1.1 Conventional X-ray analysis methods

Conventionally, researchers use Intensity equations predominantly taken from Laue and Bragg models [20]:

$$I_i^{coh} = S_F \sum_{j=1}^{N_{Phases}} \frac{f_i}{V_j^2} \sum_{k=1}^{M_{Peaks}} L_k \left|F_{k,j}\right|^2 S_j \left(2\theta_i - 2\theta_{i,k}\right) P_{k,j} A_j + bkg_i \qquad (3)$$

The above equation has lots of parameters to be defined, $S_F \sum_{j=1}^{N_{Phases}} \frac{f_i}{V_j^2}$, stands for the scale factor (S_F: Beam intensity, f_i: Volume fraction, V_j: Cell volume). L_k is the Lorentz-Polarization factor and is a function of the geometry of the sample, angle θ of the monochromator, detector, beam size, sample volume and angular position of the sample. $F_{k,j}$ is the structure factor. It is relative to the multiplicity of k^{th} reflection (m_k) and temperature factor. $P_{k,j}$ is preferred orientation and A_j is volume absorption. bkg_i is the intensity of the background which should always be known and distinguished from the intensity of the sample.

Eq. (3) is intricate and obtaining all those parameters each time for only one angle is a tedious job. Besides, Eq. (3) which is based on Laue and Bragg equations, might be a good solution for bulk crystalline materials, but in the nanoscale, it is not an

exact method [21]. DSE is a better model to describe the diffraction signature from nanomaterials and it does not require crystallinity in the materials.

1.2 Extracting characteristics of the peaks

Since the experimental peaks obtained from diffractometers are discrete data points, fitting is needed to extract the characteristics of the peaks. When analyzing X-ray diffraction data, a common practice is to model the Bragg peaks with mathematical equations since characteristic peak profile parameters can be related to average structural properties of the investigated powders [22], [23]. Two most commonly used profile functions are the Gaussian and Lorentzian profile functions.

Gaussian or normal distribution is the type of distribution that can be seen for a peak fitting and mathematically it is:

$$G(x) = \frac{1}{\sigma\sqrt{2\pi}} e^{-\frac{1}{2}(\frac{x-\mu}{\sigma})^2} \quad (4)$$

where σ is the standard deviation, μ is the mean of the distribution and σ^2 is the variance. Figure 1 shows the Gaussian fit for the third peak (pertaining to the 220 reflection) of the simulated intensity profile from 5 nm size spherical gold nanocrystal when an X-ray wavelength of 1.0 Å was assumed:

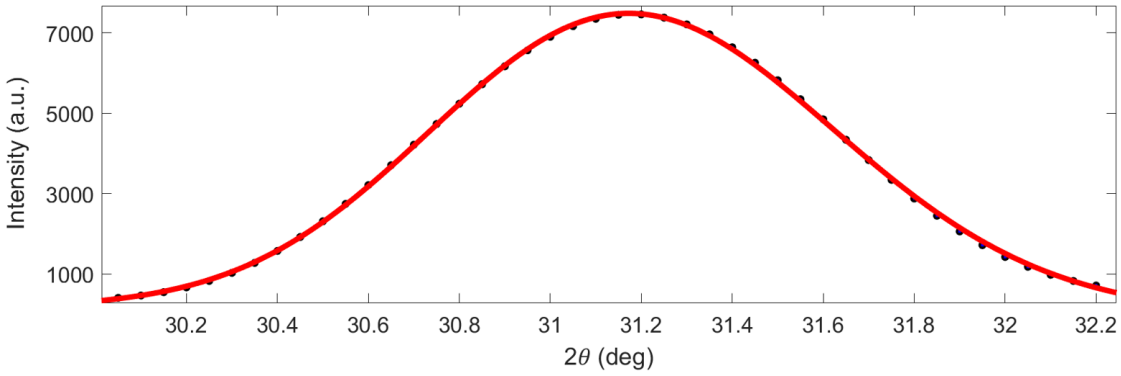

Figure 1 The Gaussian fit for the 220 diffraction peak of 5 nm spherical gold nanocrystal. Markers shown in black, are the discrete intensity data, and the red fitted line is the Gaussian fitted line.

Figure 1 is a Gaussian fitted line shown in red, and the discrete intensity data are shown in black dots. Eq. (4) is implemented to obtain the fit.

Peak fitting is highly sensitive to the resolution of data points and if there are not enough points for each peak, the fit will not be reliable as it will show the maximum intensity, 2θ and Full Width at Half Maximum (FWHM) based on the fit. In Figure 1, the minimum of the intensities is taken to be zero and the fits are done in the software "Origin Lab" for the ease of use. This is an example of a successful fit, because the red line crosses each data point. One criterion for a successful is the residual of the fit which is defined in terms of the difference between the y-coordinate of the fitted line and the data points. Residual will be discussed in detail in this chapter.

The second type of mathematical model commonly used to fit experimental Bragg peaks is the Lorentzian function [24], [25].

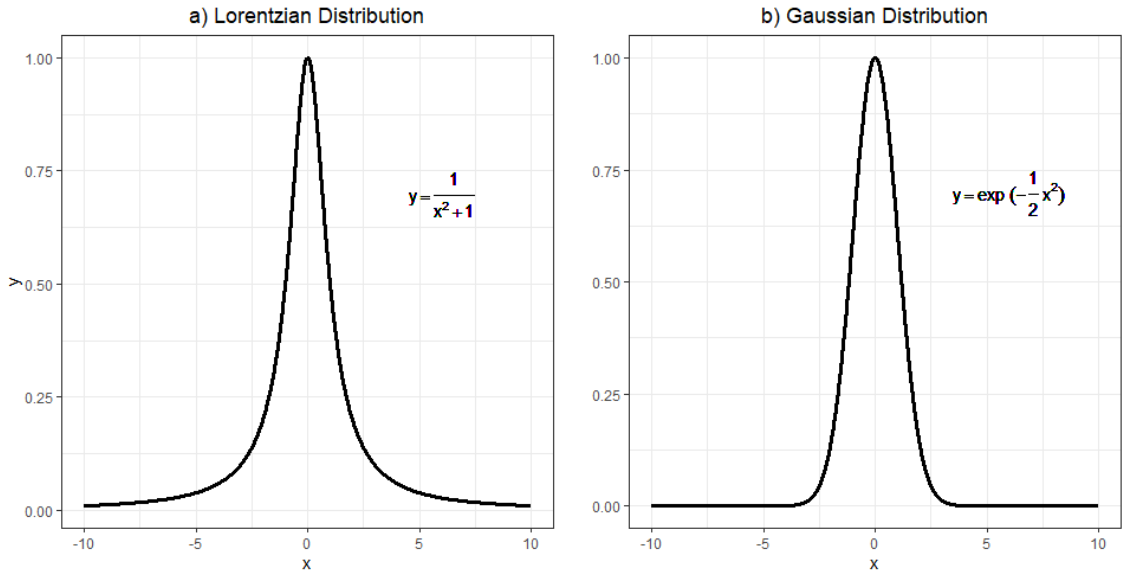

Figure 2 Normalized **a)** Lorentzian Distribution, and **b)** Gaussian Distribution in the range of x = (-10, 10).

Figure 2 shows normalized Gaussian and Lorentzian distributions with coefficients of 1 (unity). Lorentzian Distribution in fact, has the following shape:

$$L(x) = \frac{1}{\pi}\frac{\frac{1}{2}\Gamma}{(x - x_0)^2 + (\frac{1}{2}\Gamma)^2} \tag{5}$$

Γ is the width of the Lorentzian peak and x_0 is the center. In Figure 2a, the center of the peak is at x = 0, and the width of the peak (Full Width at Half Maximum [FWHM]) is 2. Knowing this, and normalizing the peak, simplification of the coefficients in Eq. (5), will yield Figure 2a. The area under both peaks in Figure 2 is:

$$\int_{-\infty}^{+\infty} L(x)dx = \int_{-\infty}^{+\infty} G(x)dx = 1 \quad (6)$$

For the Gaussian Distribution, from Eq. (4) the peak width can be obtained as:

$$FWHM = 2\sqrt{2ln2}\,\sigma = 2.355\,\sigma \quad (7)$$

In Figure 2b, the peak properties are normalized, and the coefficients are simplified, the equation shown in this figure illustrates a simplified and normalized version of the Eq. (5). The Lorentzian peak has a narrower width at its half maxima. While the Lorentzian peak has a wider base, the Gaussian peak is tighter in its base compared with the Lorentzian peak. Figure 2 shows two of the most important peaks used in X-ray diffraction, and based on the needs of each case, also based on different residuals, the best possible model can be fitted. In our research, both Gaussian and Lorentzian peaks can be fitted to PDF peaks in order to obtain the characteristic properties of the peaks and consequently, the nanocrystals. Also, diffraction patterns can be fitted to obtain the properties of the nanocrystals and compare the PDF with diffraction methods. For instance, after fitting the intensity pattern peaks to Gaussian or Lorentzian peaks, the size of the nanocrystals can be obtained and compared with the size obtained from PDF, using Scherrer equation. These will be explained in more detail in Chapter III.

1.3 Scherrer equation

Scherrer equation relates the breadth of diffraction peaks to the size of the nanocrystals. Yet, there would be different peak width values if the peak fitting process includes background subtraction. As a result, the choice of the background is another critical factor. In Figure 1, the left side of the peak is higher than the right side. There would be different peak breadth values for either side of the peaks as a peak background. However, if fitted together, the minimum of the total data can also be a good option for the background. Also, whether the peaks are fitted all at once, or each n peaks together (n is a natural number), or each of the peaks one by one, has different results. The Scherrer equation [14], [26] can show the relation of peak width and the particle size (nanocrystalline diameter) as:

$$D = \frac{K\lambda}{B\cos\theta} \tag{8}$$

where K is a dimensionless parameter called Scherrer constant and it is usually a value around unity [27]. λ Is the wavelength and B is the breadth of the peak. As B is calculated in radians, the denominator is in the order of hundredth or maybe thousandth of unity, which has a direct impact on the resulting total number. As the denominator of Eq. (8) is a small number compared to unity, a slight change in it, would make a great change in the calculated nanocrystalline size. That is why fitting the diffraction pattern with the least possible residual is a must, but there is no way to make the residual exactly zero.

1.4 Surface to Volume atom ratio, the motivations for PDF

As already mentioned, conventional X-ray diffraction methods assume perfect crystallinity for the diffracting samples [2], [28]–[30] as depicted in Eq. (3). Surface to Volume (STV) atom ratio is an important factor in X-ray diffraction that can have an adverse effect on the crystallinity of the particles [31]. The concept of STV atom ratio can be explained by the Rubik's cubes:

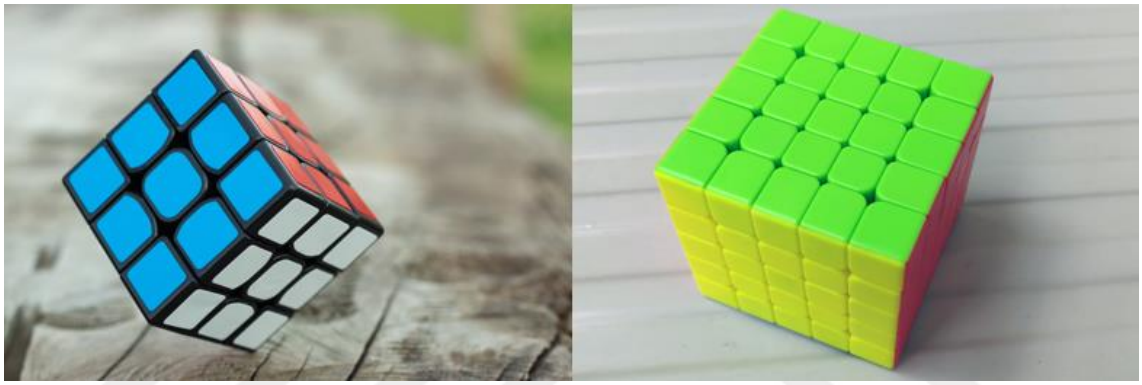

Figure 3 Rubik Cubes, left, 3×3×3 elements. Right, 5×5×5 elements [32], [33]**.**

STV ratio of a Rubik's cube is the ratio of the elements that touch the ambient environment with at least one of their faces. As a result, the STV ratio for the left cube is $\frac{26}{27}$ and for the right one, is $\frac{98}{125}$. The smaller Rubik's cube has an STV ratio which is very close to unity, while this ratio decreases for the bigger (right-side) Rubik's cube. This example clarifies the inverse relation of the STV atom ratio with particle size. Knowing the mathematical terms for the surface and the volume of a sphere:

$$STV = \frac{4\pi r^2}{\frac{4}{3}\pi r^3} = \frac{3}{r} \quad (9)$$

as can be seen, STV atom ratio for spherical shapes is inversely related to the radius of the shape. Nanocrystals are assumed to be mainly spherical in this research, unless it is stated that the shape is not spherical (i.e., shell, core and shell, elliptic, etc.). Therefore, this concept is also applicable to our spherical nanocrystals.

Another concept worth mentioning, is Coordination Numbers (CN). It is the number of nearest neighbor atoms that surround an atom. For instance, we know gold has an FCC structure with lattice parameter of 4.07825 Å [34]–[36] in its Crystallographic Information File (CIF), and its CN is 12, meaning when ideally periodic and surface effects are absent [37], [38], there are 12 other atoms surrounding each gold atom. However, for the surface atoms CN is not 12, which makes surface atoms lack restrictions in some directions and not obey crystallinity.

As already mentioned, conventional diffraction methods are highly based on the crystallinity of the structure. However, nanocrystals, because of their high STV atom ratio which leads to a dominant number of atoms that lack CN, cannot satisfy the crystallinity. That is the main motivation to think of PDF methods since they are generally applicable to both crystalline and amorphous materials [2], [21], [39].

1.5 Refinement parameters

In our research, PDF refinement is the process of obtaining the parameters of the nanocrystals by refining the parameters initially entered by the user or obtained from the

CIF files. We do refinement to obtain the morphological parameters of the nanocrystalline structure. Nanocrystals do not necessarily have the same properties as their bulk counterparts [40]–[42]. Least squares method is vastly used in our refinements [43]. The parameters to refine in this research, mostly consist of lattice parameter, particle size, scale factor, and Atomic Displacement Parameter (ADP). Lattice parameter is the physical dimension of the crystal lattice that defines the unit cell [44]. Lattice parameters consist of interplanar angles and lengths of the atomic unit cells. Unit cells are the smallest group of atoms that the entire structure can be made by repeating them. Unit cells have 3D parameters, 3 dimensions (a, b, and c) and 3 angles (α, β, and γ). For gold nanocrystals, the unit cell has the same length in all the axes. As a result, lattice parameter for gold nanocrystals is shown by "a" which is numerically 4.07825 Å. It has a Face Centered Cubic (FCC) structure, and all angles are 90°. An FCC unit cell is shown in Figure 4:

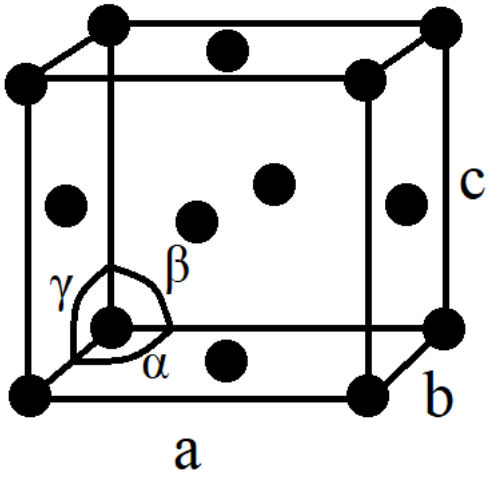

Figure 4 FCC unit cell with lattice parameters in three different dimensions. The black circles represent gold atoms.

Particle size is the maximum interatomic distance found in the nanocrystalline structure. In PDF fitting process, the initial lattice parameter is read from the CIF file. When fitting the bulk shape to the nanocrystalline PDF pattern, the intensity of the peaks change with a scale called scale factor [45]. ADP consists of both temperature-induced and temperature-independent displacements of the atoms from their lattice points [46]. To understand the ADP, there are some other parameters to introduce; Instantaneous atomic displacements are shown as "u", the average of their square is shown by $U = \langle u^2 \rangle$. In another words, Root-Mean-Square (RMS) of displacements is the square root of U. ADP is sometimes shown as B parameter. B and U are related to the Debye-Waller factor and have the following relation [47]:

$$B = U.8\,\pi^2 \tag{10}$$

1.6 Fourier Transform

Pair distribution function analysis is based on Fourier transforming the measured diffraction data since it is assumed that the transformed diffraction data can be related to the interatomic spacing histogram in the irradiated crystallites [2], [48]. In order to obtain the PDF from X-ray diffraction (which means to bring the data from reciprocal space to the real space), we need to utilize Fourier transform as in Eq. (11). If "F" is an integrable function, and $\omega = n\omega_0$, while n is an integer and $\omega_0 = \frac{2\pi}{T}$. T is the period of the function f(t) [49]:

$$f(t) = \frac{1}{2\pi}\int_{-\infty}^{+\infty} F(\omega)e^{i\omega t}d\omega \tag{11}$$

$$F(\omega) = \int_{-\infty}^{+\infty} f(t)e^{-i\omega t}dt \tag{12}$$

Eq. (11) can be used to change the diffraction pattern of reciprocal space into real space PDF data. It has a range of (-∞,+∞), but in experimental diffraction measurements, the ranges of the integral are $\vec{Q}_{\min}$ and $\vec{Q}_{\max}$ which are related to the minimum and maximum possible magnitudes of the scattering vector for the X-ray diffraction by $\left|\vec{Q}_{max}\right| = \frac{4\pi \sin\theta_{max}}{\lambda}$ and $\left|\vec{Q}_{min}\right| = \frac{4\pi \sin\theta_{min}}{\lambda}$. This change of the range from infinity to finite amounts will cause a trouble called termination ripples [2], [50] which will continue to exist in the PDF peaks and might be mistaken for real peaks (Here PDF peaks are not intensity peaks of the diffraction data but the peaks of the interatomic histograms for the irradiated crystallites). This would be debated in the coming parts and the possible solutions will be mentioned using an example for better comprehension.

1.7 The main Concept

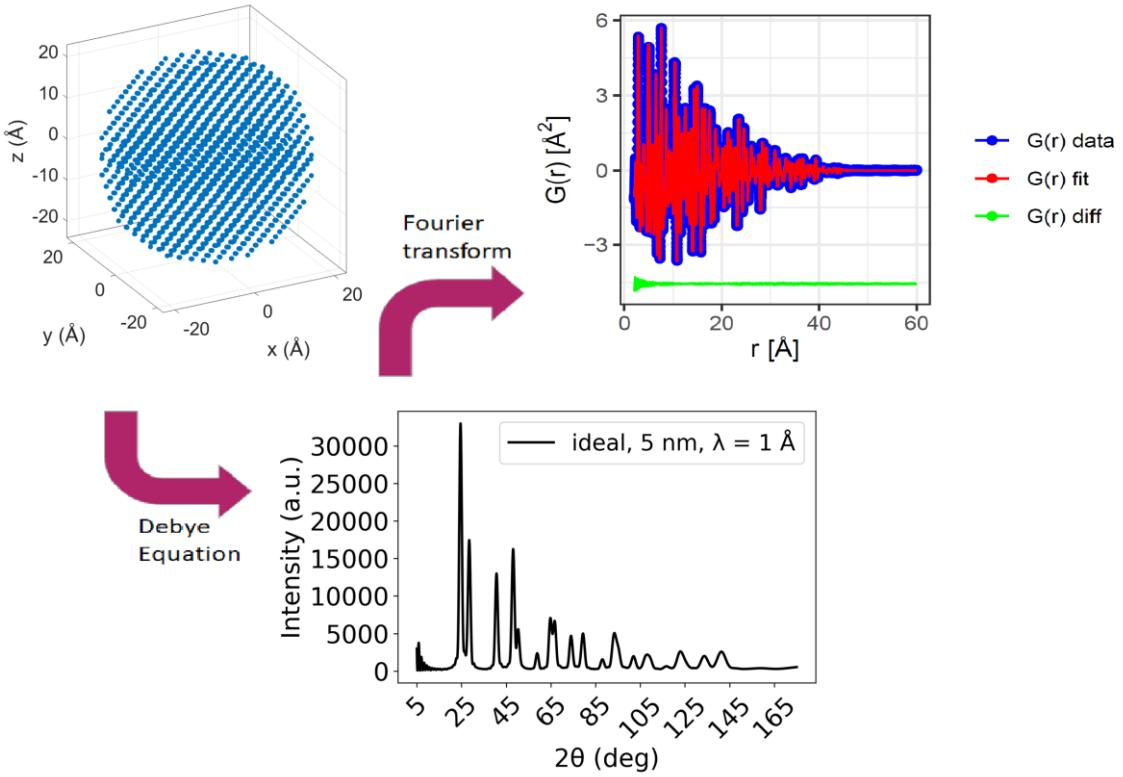

Figure 5 Schematic of the workflow involved in PDF analysis for the 5 nm ideal nanocrystalline. Ideal nanocrystals are not treated with molecular dynamics simulations.

The whole process of this dissertation is depicted in Figure 5. It illustrates the main concept and workflows done in this research and shows how the 3D coordinates of a group of atoms can be converted to their PDF data using the Debye equation to create simulated diffraction datasets followed by Fourier transforms.

Starting from the input file (3D coordinates of atoms) at the top left of the Figure 5, Debye equation is calculated, which results in the diffraction pattern. The diffraction

pattern shows the Bragg peaks of the X-rayed powder and their angular distributions. It is an “Intensity vs. 2θ” file of information. Diffraction patterns are in reciprocal space [$Å^{-1}$]. To obtain their PDF, Fourier transformation is applied. The top right subfigure of Figure 5 shows the PDF of the 5 nm nanocrystal shown in the top left of the figure. Diffraction pattern acts as a transition from 3D coordinates to the PDF pattern.

There are different parameters that can be obtained from PDF data, including particle size, particle shape, lattice parameters, coordination number, phase of the material or the components comprising the material, etc.

Particle size can be obtained from the attenuation of the PDF peaks, because there would be no probability of finding atoms at distances more than particle size. Shape of the particle needs a shape factor (see Appendix D for shape factor equations). Before doing PDF analysis, one can visualize the 3D coordinate of the particle to have an initial assumption about the shape of the particle. Coordination number can be obtained from the area (width and amplitude) comparison of the PDF peaks. Usually the interatomic distance histogram has the maximum amplitude for the peak corresponding to the smallest interatomic distance [2], [51], [52]. Lattice parameters and strains are refined using least squares method.

1.8 The calculations of PDF

Statistically, PDF is the relative probability of finding two atoms at a distance “r” with the thickness of “dr” from each other. Based on the thickness of “dr” and the interatomic distance “r”, there are different amplitudes and thicknesses for each peak [53]. The principal rule for doing so, is to locate one atom and do the PDF calculations (Eq. (13)) based on the same atom:

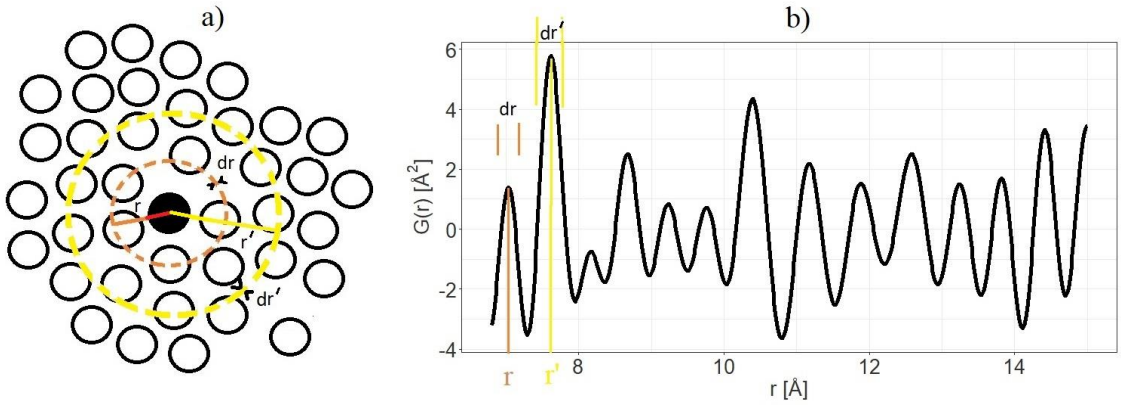

Figure 6 a) The probability of finding any atoms around the central atom at distances r and r'. The central atom is fixed, thicknesses are different. **b)** the PDF pattern of the probabilities in part a. The central atom is colored in black.

Figure 6a shows the atoms found at distances r and r′ around the central atom in the middle of the circles. These probabilities have a thickness as well. Finding atoms at those positions will result in the PDF pattern seen in Figure 6b. The concept of local interatomic measurement is clearly shown in Figure 6. Each interatomic distance (r) is related to a peak in the PDF pattern. ADPs are directly related to the width of the peaks.

One of the main challenges in characterization of nanomaterials is obtaining the exact position of the atoms in three dimensional spaces [31]. A very important approach to solve this issue is addressed by the concept of PDF which is a list of interatomic distances [2], [54]. After doing X-ray or neutron diffraction on the samples, the diffraction data can be turned into structure function and can be Fourier transformed to obtain the PDF. A big challenge in determining the interatomic distance in PDF, is the vectors with the same length that overlap. That is why peak fitting is an important process to address that problem. A structural model is needed for fitting the PDF data

obtained from diffraction measurements. This is the real-space equivalent of the Rietveld method[1] [55], [56]. Obtaining the refined parameters without fitting a structural model to the data is impossible.

To define the PDF, consider a nanocrystalline particle with a total number of atoms N in it [2], [48], [57]–[59]:

$$G(r) = \frac{2}{\pi}\int_{0}^{+\infty} F(Q)sin(Qr)dQ \approx \frac{2}{\pi}\int_{Q_{min}}^{Q_{max}} F(Q)sin(Qr)dQ \qquad (13)$$

In fact, Q_i is discrete, and the above equation can numerically be calculated as below:

$$G(r_j) \approx \frac{2}{\pi}\sum_{i=1}^{N_Q} F(Q_i)sin(Q_i r_j)\Delta Q_i \qquad (14)$$

N_Q is the number of discrete values of Q, and ΔQ_i is the step size or $\Delta Q_i = Q_{i+1} - Q_i$. F(Q) is the reduced structure function [53]:

$$F(Q) = Q[S(Q) - 1] \qquad (15)$$

S(Q) is the normalized scattering intensity from a sample [53]:

[1] Hugo Rietveld described Rietveld refinement method as an interpretation of X-ray or neutron diffraction pattern of crystalline materials [103], [104].

$$S(Q) = \frac{I(Q) - \langle f^2 \rangle + \langle f \rangle^2}{\langle f^2 \rangle} \quad (16)$$

I(Q) is the intensity of the diffraction pattern as a function of momentum transfer vector (Q). $\langle f \rangle^2$ is the square of the angular-averaged scattering factor, and $\langle f^2 \rangle$ is the average of the squared scattering factor. It means that firstly, the square of all the scattering factors is calculated, then the numerical average of them has been calculated. While Eq. (13) calculates the PDF from reciprocal space of diffraction pattern, Eq. (17) does the same in real space:

$$G(r) = 4\pi r[\rho(r) - \rho_0] \quad (17)$$

$\rho(r)$ is the real space pair density, and ρ_0 is the number density. Each crystal lattice has its own characteristic number density. For example, Gold, theoretically has a number density of 10.21 $cm^3.mol^{-1}$ [60] In fact, this value (10.21 $cm^3.mol^{-1}$) is the molar volume which is the reciprocal of the number density with the unit of [$mol.cm^{-3}$]. Number density is different than the mass density which the volume of [$g.cm^{-3}$]. Figure 7 helps to distinguish between number density and mass density:

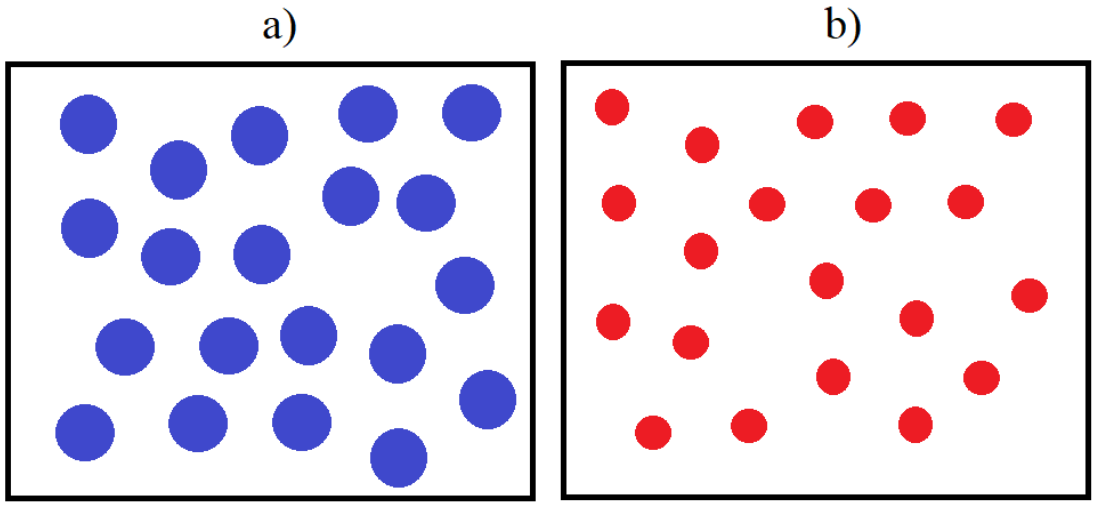

Figure 7 Number densities of two materials. **a)** larger atom sizes. **b)** smaller atom sizes.

Figure 7 shows two different materials with the same number of atoms. Figure 7a has larger atom sizes, while Figure 7b has smaller atom sizes. Both of the subplots have the same number density, while the mass density of the Figure 7a is bigger than Figure 7b because of bigger atoms (possessing a heavier mass).

Below equation yields $\boldsymbol{\rho}(\boldsymbol{r})$ in a radial distance "r" from the central atom in Figure 6a [57]:

$$\rho(r) = \frac{1}{4\pi R^2 N} \sum_{i=1}^{N} \sum_{j=1,j}^{N} \frac{f_i f_j}{<b>^2} \delta(r - r_{ij}) \qquad (18)$$

As mentioned, ρ_0 is the average number density of the material which is a constant number. Atomic number density can be defined as the total number of atoms per unit cell.

In Eq. (18), $\rho(r)$ is the mean weighted density of the neighbor atoms from an atom in the origin. f_j is the scattering factor of atom j and <f> is the average scattering factor [61]. r_{ij} is the relative distance between atoms i and j.

The PDF of a nanocrystal is different from the PDF of the bulk materials [45], [48], [62]. In nanomaterials, the PDF peaks get attenuated as r increases, while in bulk materials, the PDF does not necessarily attenuate. The reason for attenuation is the fact that there is no probability of finding a pair of atoms at the distances which are bigger than the particle size. The function that does the attenuation for the nanocrystals is called "Shape function" [63] and it is unique for each particle shape. Usually, integral equations are used for obtaining the shape functions, but for the simple shapes like spheroids, core and shells, rods, etc., they can be obtained analytically [51], [63].

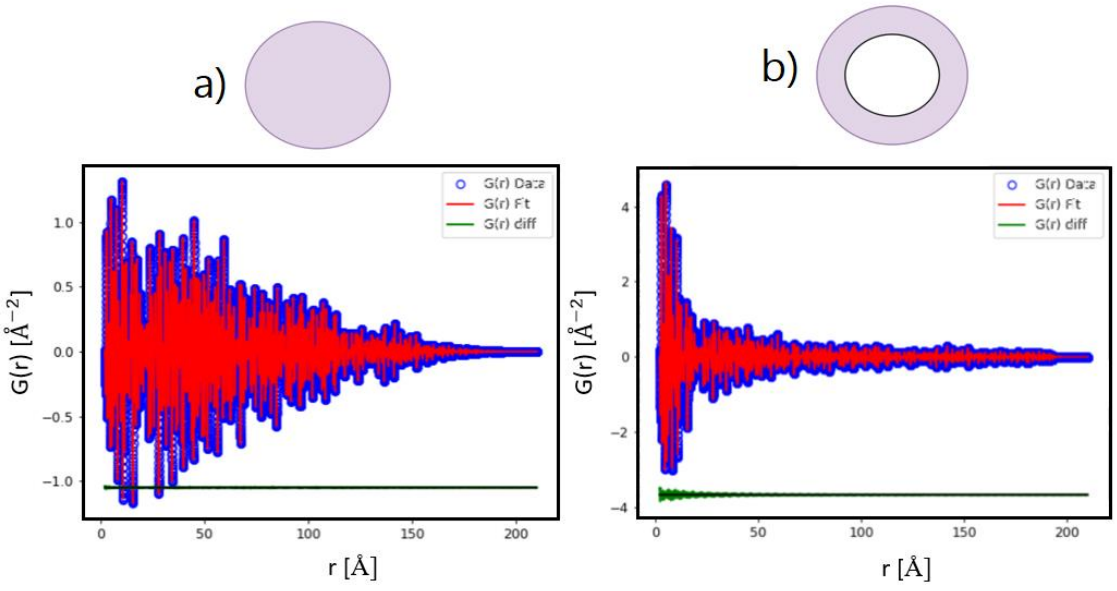

Figure 8 Impact of the nanocrystal shape on the corresponding Pair distribution functions, **a)** Spherical particle and **b)** Shell particle.

Figure 8 shows the importance of the shape in PDF. If the shape function is wrong, the PDF will not get fitted. In Figure 8, the PDF shows a very intuitive characteristic of a nanomaterial, when there is a spheroid (Figure 8a), the peaks are decreasing gradually, meaning as r gets bigger, the probability of finding a pair of atoms at that distance decreases and this happens gradually because of the geometry of the sphere. In contrast, when we have a spherical shell [hollow sphere] (Figure 8b), the PDF will decrease drastically after a distance (which is the thickness of the shell). Beyond that distance, the PDF peaks lose their intensity and will have an almost constant intensity, because the probability of finding a pair of atoms at that distance becomes almost the same, no matter how r increases. The reason behind this is the circular symmetry of the crystallite geometry. The blue dots in Figure 8 show the experimental PDF obtained from measurements (diffractometer or synchrotron). The red line is the fitted PDF model. The fitted line starts from the CIF file and uses least squares method to get fitted to the blue dots. The difference of blue dots and red fitted line is shown as the green line and is known as the residual of the fit. Residual can be shown as [2], [64]:

$$Rw = \sqrt{\frac{\sum_i [\omega_i (g(r_i) - g_{calc}(r_i))]^2}{\sum_i \omega_i [g(r_i)]^2}} \tag{19}$$

where g is the experimentally obtained PDF (blue dots) and g_{calc} is the fitted red line. ω_i is the weight with uncertainty of the values. $\omega_i = 1/\sigma^2[g(r_i)]$. σ is the uncertainty of the refined parameters [65]. There is also another method called R-squared (R^2):

$$R^2 = 1 - \frac{\sum_{i=1}^{N}(g(r_i) - \bar{g}(r_i))^2}{\sum_{i=1}^{N}(g_{calc}(r_i) - \bar{g}_{calc}(r_i))^2}\ , 0 < R^2 < 1 \qquad (20)$$

$g(r_i)$ is the y-coordinate of the raw data points, $\bar{g}(r_i)$ is their mean. $g_{calc}(r_i)$ is the y-coordinate of the fitted points, and $\bar{g}_{calc}(r_i)$ is their mean. The maximum possible amount for R^2 is 1 which means perfect fitting. R^2 method is pervasively used method in regression models [66]–[68]. However, Rw resembles Mean Absolute Value (MAE) method [69]. Both of these methods are used in this research to evaluate the goodness of fits of the analytically-modeled PDFs to the PDFs obtained from diffraction data.

CHAPTER II

CREATION OF SIMULATED DIFFRACTION DATASETS

In X-ray diffraction, the usual input data (as in Figure 9) is an atomic coordinate file containing a high number of atoms as below:

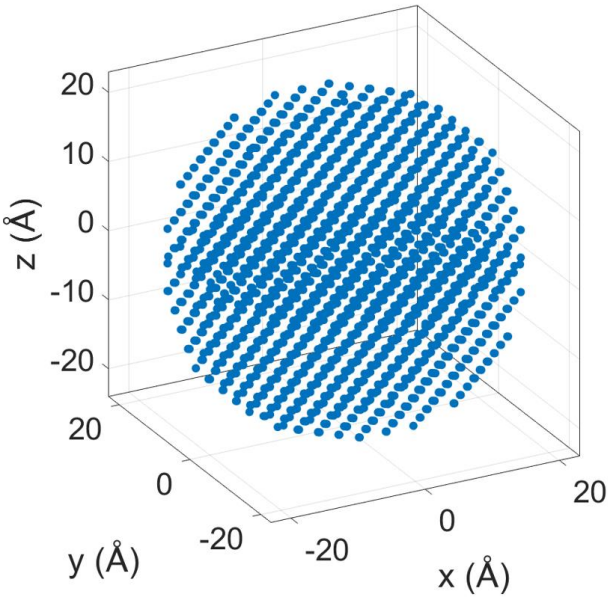

Figure 9 Input data shown in 3D mode. The data consists of 3589 atoms and units are in Angstrom. Each blue sphere corresponds to an atom in the nanocrystal.

Positions of the atoms are taken as the input files. Usually they have a ".xyz" format. Debyer [70] is the software that has been used in order to obtain intensity files out of atomic coordinate files. Based on the commands given, debyer will produce the intensity file. For instance:

$ debyer -x -f1 -t180 -s0.01 --quanta=0.0001 -l1.5418 -o OUTPUTFILENAME INPUTFILENAME

The above commands will take the atomic coordinations with the name "INPUTFILENAME" and return an intensity file with the name "OUTPUTFILENAME". "debyer" calls the software name for the operation, "-x" stands for X-ray scattering, "-f" is the abbreviation of the word, from, (a degree to start diffraction from), "-t" means to (to the degree which scattering is going to end), "-s" is step size (in degrees), "-l" stands for wavelength of the incoming wave and "-o" means output file name. Quanta is the interatomic distance discretization quanta, and it is 0.001 by default. Using debye scattering equation, debyer makes histograms of interatomic distance vectors r_{mn} to optimize the computation time. Quanta is a determining factor for the accuracy of the calculated intensities, so it must be chosen with great consideration. In our study, a histogram width of 0.0001 Å has been tested and the resulting errors were confirmed to be negligible for all of the nanocrystals investigated.

A usual output of debyer for a particle of 28897 atoms of gold with approximate diameter of 10 nm, under a wavelength illumination of 1.5418 Å, is seen in Figure 10. This figure shows the orientationally averaged intensities of constructive Bragg reflections [Eq. (1)] as peaks with different amplitudes evaluated by Eq. (2). Bragg's law can always be implemented to check the data [Eq. (1)]. For the fist peak in Figure 10, we have:

$$2d \sin\theta = \lambda$$

$$2d\sin(12.3\ deg) = 1\ \text{Å}$$

$$d = \frac{a}{\sqrt{h^2 + k^2 + l^2}} = \frac{4.078}{\sqrt{h^2 + k^2 + l^2}} = \frac{1}{2.\sin(12.3\ deg)} = 2.35$$

$$\sqrt{h^2 + k^2 + l^2} = 1.7376$$

$$(hkl) = (111)$$

Which is true, based on the allowed and forbidden reflections from FCC crystal structures (see Appendix C). Each peak in Figure 10 is related to an angle of reflection from an interplanar distance which is predictable by Bragg's law [Eq. (1)].

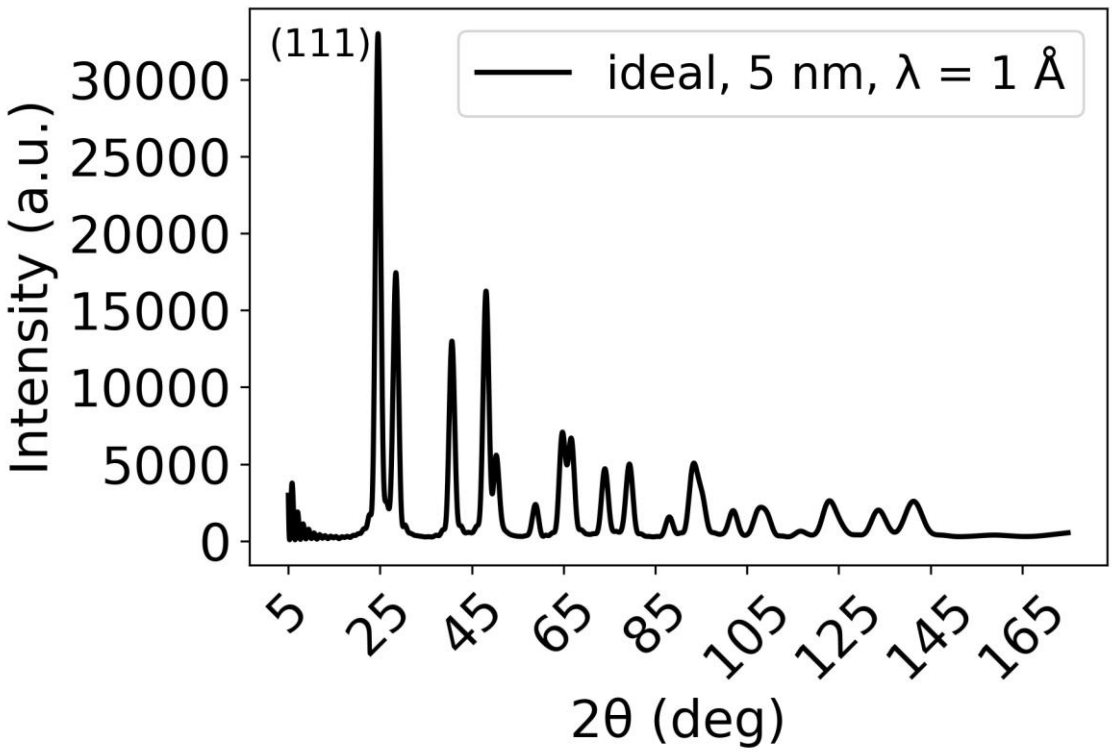

Figure 10 Output of "debyer" package as an intensity file from the atomic coordinate file for the ideal 28897 atoms of gold from 5 to 180 degrees with wavelength = 1.0 Å. As shown at its top, the first peak is related to the reflection from (111) plane.

There are two different categories of atomic coordinate files in this research, one is directly obtained from positions of the lattice structure, without any Molecular Dynamics (MD) analysis. We call these particle models the ideal crystalline Gold nanoparticles. The second is the atomic coordinate file obtained from Molecular Dynamics simulations where the total energy of the nanoparticle was minimized at different temperatures and 1 standard atmosphere pressure. The MD based atomic coordinate files were obtained by Merdan Batyrov, a PhD student in our group. Figure 10 shows the diffraction results for the atomic coordinate file without MD refinements.

The next step is to turn intensity files to PDF using mentioned equations and the software PDFgetX3 [71]. An example command is shown in Appendix A.

After obtaining the PDF data using PDFgetX3, data must be fitted in order to obtain the characteristic parameters like ADP's, Lattice Parameters, Particle Size, etc. For a PDF fitting, Diffpy-Complex Modeling Infrastructure (CMI) [72] which has a Python-based coding environment is utilized [61], [64], [72]. The software takes the PDF output of PDFgetX3 as an input and using a CIF file, it will provide fits for its input. The PDF fitting is sensitive to many parameters and changing the initial values will have impacts on the refined values. As Diffpy-CMI has a coding environment, one can have much freedom in presenting the outputs and/or saving them for future use. The package is free of charge for academic use [72].

As mentioned, after using PDFgetX3, the intensity files will change to the PDF files. These data are shown as G(r) data which will be conventionally shown as scattered dots in Diffpy- CMI.

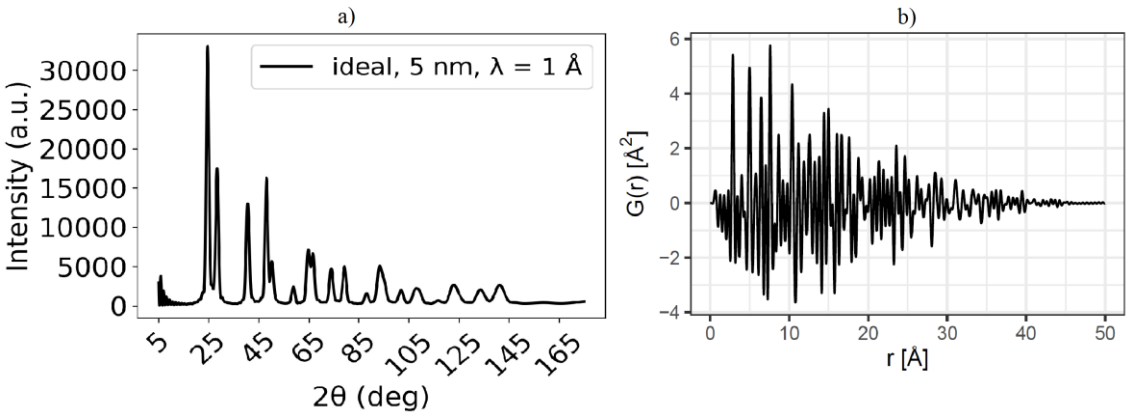

Figure 11 a) Diffraction pattern as an input to PDFgetX3, and **b)** PDF pattern as the output of the PDFgetX3. The nominal particle size is 5 nm at ideal conditions, illuminating X-ray wavelength is 1 Å.

Figure 11b shows a simple output of PDFgetX3 with a resolution of dr = 0.01 Å. The horizontal axis which is r [Å] is the interatomic distance and the vertical axis is the probability of finding a pair of atoms at that distance. These concepts have already been mentioned in the introduction part mathematically. The PDF which is shown by G(r) in the graphs is the amount of the PDF probability and based on Eq. (13), has a unit of [$Å^{-2}$]. From Figure 11b, it can be realized that there are finite probabilities of finding atoms at distances less than 50 Å, because the amplitudes of the probability peaks are positive and nonzero. Anywhere that the peaks are significantly attenuated can be interpreted as the particle size [73]. The material is gold and has an FCC structure which has its nearest neighbor distance of $\frac{\sqrt{2}}{2}a$, where "a" is the lattice parameter of gold. At standard conditions, the lattice parameter mentioned in the CIF files for gold nanocrystals is 4.078 Å. As a result, the nearest neighbor distance for a gold nanocrystal is $\frac{\sqrt{2}}{2}(4.078)$=2.88 Å.

CHAPTER III

SYSTEMATIC ANALYSIS OF DIFFRACTION DATA FROM GOLD NANOCRYSTALLINE POWDERS

In this chapter, the results of the PDF fitting is illustrated and the analysis and interpretation of the refined parameters have been discussed.

Figure 12 is the close-up range of PDF for gold nanocrystals between r = 2 to r = 10 Å from Figure 11.b:

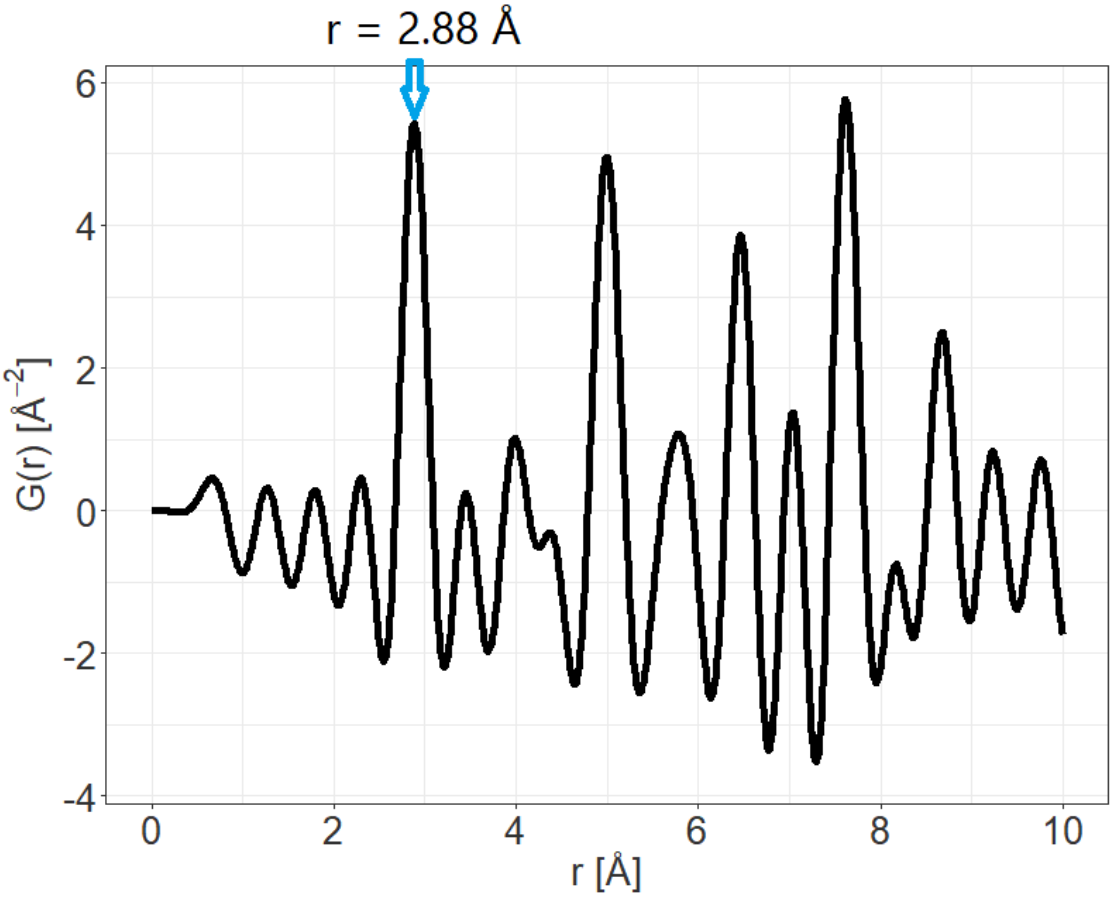

Figure 12 PDF of the ideal 5 nm gold nanocrystal in (2-10) Å. As it is anticipated, the first peak is occurring at r = 2.88 Å.

Figure 12 shows the ideal 5 nm gold nanocrystals PDF in (2-10) Å. These data are discrete and need to be fitted. The figure verifies the calculations done around the first neighboring atoms which exactly have the distance of 2.88 Å. The second nearest neighboring atoms are at r = 4.078 Å distance, and so on. The following is a table showing all the available neighboring distances less than 10 Å and they have been calculated mathematically from the geometry of the gold unit cell. In fact, Table 1 presents the center position of the peaks shown in Figure 12.

Table 1 The neighboring atom distances of less than 10 Å for the gold nanocrystal in Figure 12.

Peak order	Expected interatomic distances for Gold crystallite (Å)
1st	2.88 Å
2nd	4.08 Å
3rd	4.97 Å
4th	5.75 Å
5th	6.42 Å
6th	7.87 Å
7th	8.125 Å
8th	8.61 Å
9th	9.08 Å
10th	9.53 Å
11th	9.95 Å

Figure 12 and Table 1 agree on the positions of all PDF peaks. There are also other peaks and valleys in Figure 12. The valleys might not seem statistically meaningful, but they can be comprehended as no probability of finding two atoms at those distances. In Figure 12, peaks at r = 2.32 Å and r = 3.46 Å can be found that occur

periodically through the whole "r" range, which are called termination ripples and they are found as a result of the Fourier transformation of the intensity file to the PDF. Termination ripples are found because of the Fourier transformation being performed within a limited angular range as shown in Eq. (13). In fact, what the softwares take in as the angular ranges are not infinite. Eq. (13) described it very well that the ranges are theoretically infinite, while in practice, they must be finite, and that is the main reason for termination ripples. Termination ripples have a characteristic width that can be obtained from below equation:

$$\sigma \approx \frac{2\pi}{Q_{max}} \tag{21}$$

Where σ is the width of the termination ripple, and Q_{max} is the largest magnitude of momentum transfer vector available from the angular range of the diffraction data. Termination ripples are not noise. If Q_{max} is not high enough, the oscillations of the structure cannot be distinguished from termination ripples [50], [74]. As a result, Q_{max} should be maximized during diffraction measurements to reduce termination ripples effect. In low "r" regions, ripples are easily distinguished from real PDF peaks. The reason is, in this region, the nearest neighbor peaks are of highest amplitude. Real peaks possess relatively higher amplitudes, while termination ripples have lower amplitudes. Using Eq. (21), the width of termination ripples can be obtained. Not every single oscillation in PDF carries structural information. For instance, Figure 13, is the PDF of a 5 nm ideal gold nanocrystal with an illuminating X-ray of λ = 0.71073 Å in the range (2-10) Å:

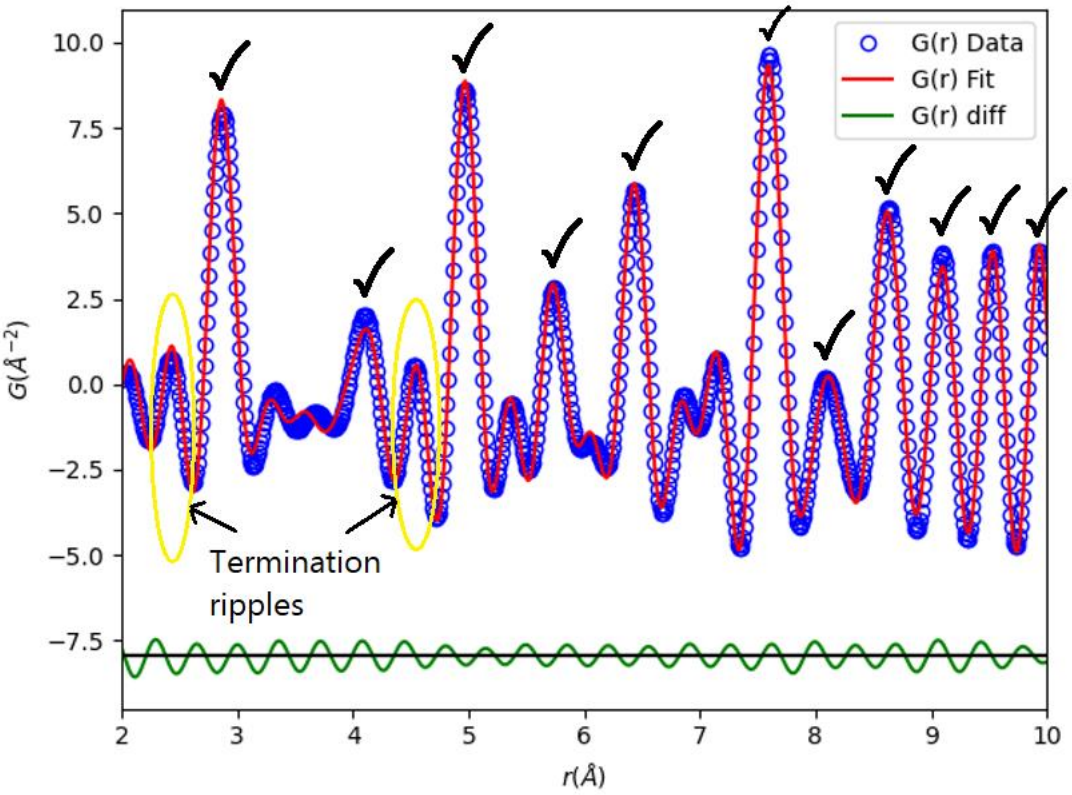

Figure 13 Fitted PDF of the ideal 5 nm gold nanocrystal with λ = 0.71073 Å in the "r" range of (2-10) Å. The first three high amplitude peaks occur at 2.88 Å, 4.97 Å, and 7.87 Å. Termination ripples are shown in yellow ellipsoids. Real peaks are marked by black ticks.

In Figure 13 termination ripples can be distinguished from the real peaks. For example, the relatively small peak between 2 and 3 Å, or the peak with the same shape and width between 4 and 5 Å, these peaks are termination ripples. The reason is:

$$Q_{max} = \frac{4\pi}{\lambda} = \frac{4\pi}{0.71073\ \text{Å}} = 17.681\ [\text{Å}^{-1}]$$

$$\sigma \approx \frac{2\pi}{17.681} \approx 0.355 \text{ Å}$$

Looking back at Figure 13, termination ripples have the same width.

In summary, PDF gives a lot of beneficial information about the structure (i.e., lattice parameter, particle size, particle shape, ADP's, phase of the material, CN, disorders, etc.) in a model independent manner [53], [75]. Structural parameters of the irradiated sample can be monitored during an in-situ XRD experiment. The fact that PDF is in real space measurements gives an intuitive understanding of the refined parameters. PDF gives orientationally averaged properties of materials, in fact, it is a histogram of interatomic distances. Thermal motion and static disorder are the parameters that can be measured from the PDF peak widths. For example, increased thermal motion of the atoms cause broadened PDF peaks and asymmetries of the peaks can be related to the surface strains [2], [76]. Also, integrating the intensity of the peaks reveals the CN of the atoms and the reason is the proportionality between the magnitude of the peaks and the number of scatterers at those distances from each other.

In order to obtain the refined parameters from the PDF analysis, Diffpy-CMI [77] is utilized to fit the best possible function to the PDF graph of Figure 13 based on Least-square Minimization (LM) fitting in Python. In coding the Diffpy-CMI [78], one should call the related fitting packages at the very first lines of the code. Packages like loadcrystal, DebyePDFGenerator, Fitrecipe, etc. each does a separate job in the PDF refinement process. For instance, the mentioned packages do the loading of the crystal structure out of the CIF file, generate the PDF graph out of the CIF file for the bulk shape of the material and make a recipe for the fit, and give a recipe for the fitting process, respectively. PDF fitting is an optimization problem, as a result, from

“scipy.optimize.minpack”, “leastsq” package is called, which is the base for this process. The idea is to find the least square of the residual and the variable values. Writing the related codes in a function will make it easier for the total process of the fitting. PDF fitting is a step-by-step refinement process. In each step, least squares method is implemented, and after making each parameter “fix” or “free” to optimize, the optimization is done. Each parameter needs to be added to FITrecipe in order to refine. There are two possibilities for a variable in a refinement. Fix or free, which respectively account for fixed variables during a refinement, or free to be refined. The Q_{damp} parameter accounts for resolution of the instrument [79]. Usually an initial value of 0.02 [80] and 0.04 is used for Q_{damp} [81], [82]. Q_{broad}, Q_{min} and Q_{max} are parameters which do not need any refinement. Writing a Diffpy-CMI code consists of three main parts: 1) Taking the inputs (CIF file and PDF file). 2) Fitting, using LM algorithms. 3) Giving the results, saving them for the possible post-processing, and sketching their graph.

There is no obligation for fitting the total range of the interatomic distances in order to obtain the properties and parameters of a material. The usual interatomic distance ranges for fitting selected in past literature is between 0 to 20-30 Å [10], [83], but in this work, the whole range of the data have been fitted because there is no background scattering, even the Bragg peaks at high angular values are resolved-enough from the diffuse scattering component. Also, showing the particle size and giving an intuitive understanding of the PDF fitting, is another reason for the whole range fits.

Figure 14 is the output of the Diffpy-CMI for an ideal 5 nm particle and shows a fitted PDF with the residual weighted (Rw) of almost %6. Figure 14 illustrates a successful fit with a low residual. Residual is not the only factor for goodness of the fit. Also, the fitted PDF model should be visually checked against the PDF of the

diffraction data and the refined structural parameters must be investigated for consistency. Usually, a residual less than 10% results in acceptable fits between the modeled and the measured PDFs.

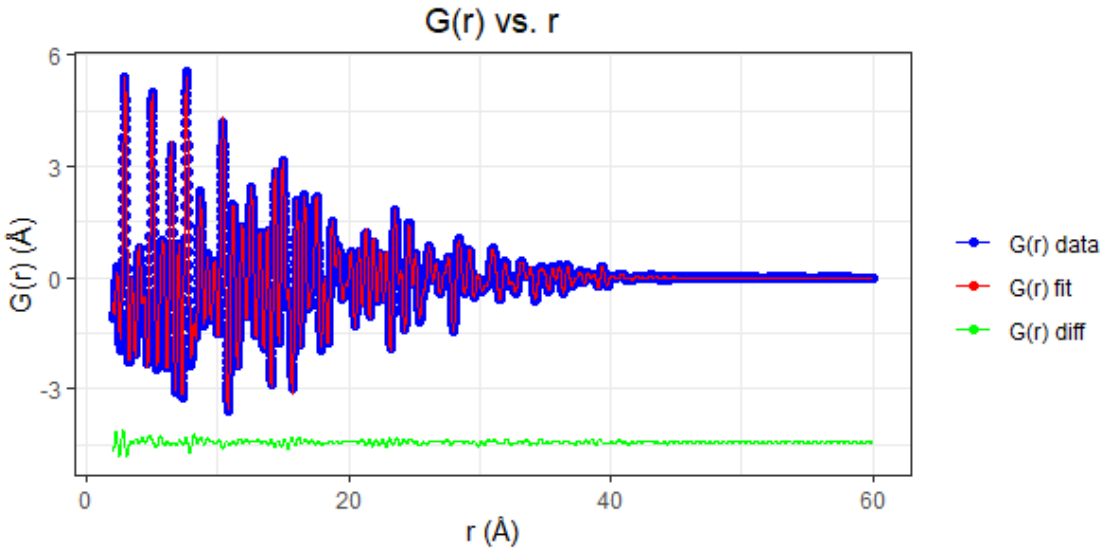

Figure 14 Fitted PDF of the ideal 5 nm gold nanocrystal. The red line is the output of the PDFGenerator package (modeled PDF) which is the fitted G(r) out of the CIF file. The blue dots are the experimental G(r) values, and the green line is their difference or residual.

As the particle size increases, the computation time of the refinement grows exponentially. The reason is because of the increased number of atoms, there are more interatomic distances to calculate the probability of finding two atoms at these distances. The finite size of the particle can be obtained using shape factors (see Appendix D). In PDF fitting, it is not possible to obtain the particle size unless having an assumption about the totality of the shape of the particle. The better the assumption about the particle shape, the more accurate the particle size. Typical shape functions

used in past literature, are Spherical (including prolate and oblate spheroids), shell, core and shell. The PDF of the bulk material is made from the CIF file, using the shape functions, the parameters change from the bulk shape PDF to the nanocrystalline shape [51].

3.1 Diffraction results of the samples

In this section we present systematic results of performance of PDF method at 5 different wavelengths, with 5 different particle sizes considering 5 different ambient conditions. Wavelengths are: 1.5418 Å, 1 Å, 0.71073 Å, 0.560871 Å, and 0.210616 Å which have the maximum momentum transfer vector (Q_{max}) of 8.151 $Å^{-1}$, 12.566 $Å^{-1}$, 17.681 $Å^{-1}$, 22.405 $Å^{-1}$, and 59.665 $Å^{-1}$, respectively. The reason we select these wavelengths is because they are related to Kα radiation wavelength of copper (1.5418 Å), molybdenum (0.71073 Å), silver (0.560871 Å), and tungsten (0.210616 Å). The nominal particle sizes are 5 nm, 10 nm, 15 nm, 20 nm, and 30 nm. Ambient conditions consist of ideal conditions (no temperature, pressure, etc. effect), and MD energy-minimized conditions at 0 K at 10^5 pascal ambient pressure.

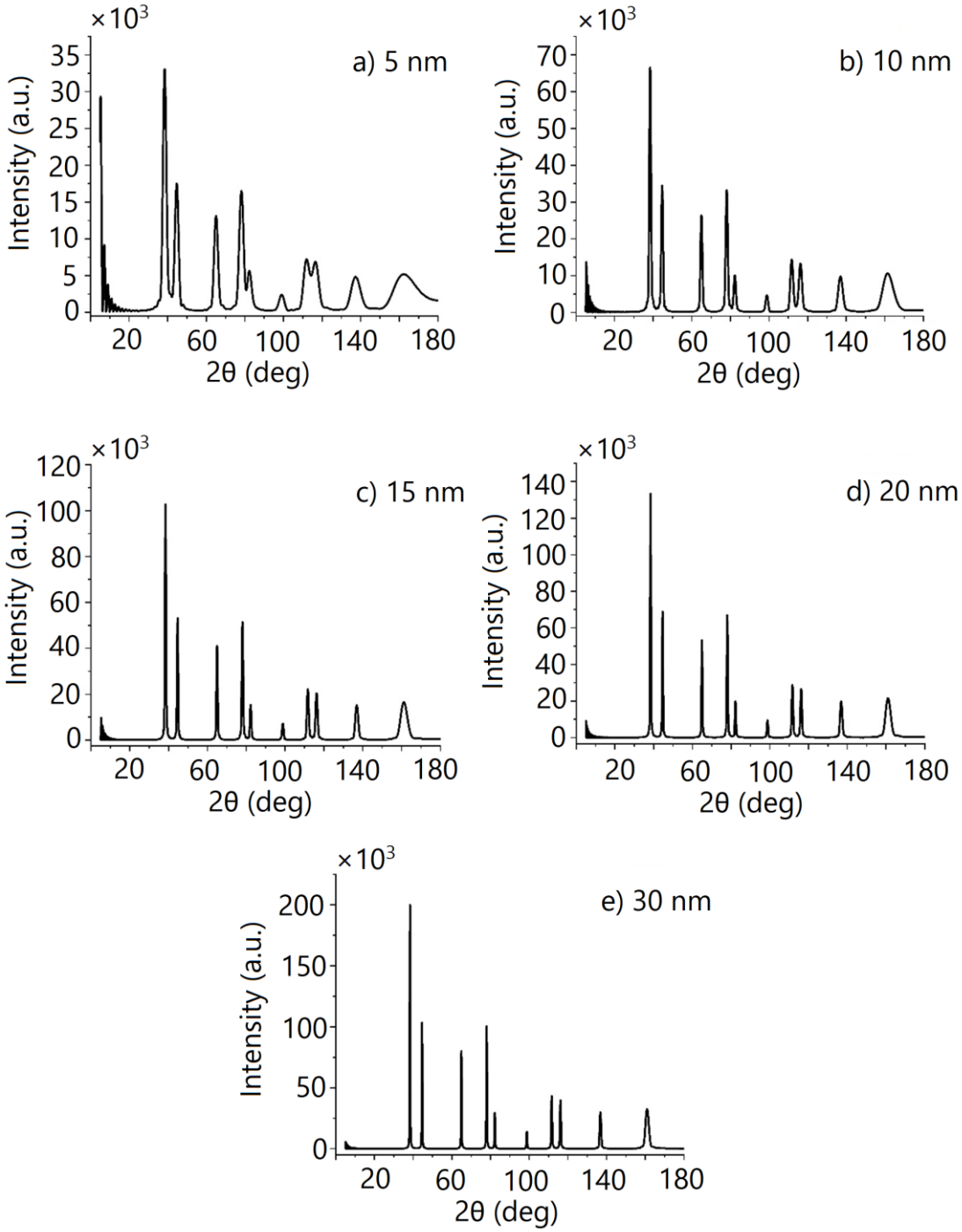

Figure 15 Angular intensity distributions of five energy-minimized spherical gold nanocrystals with different sizes (at 0 K and ambient pressure), a) 5 nm, b) 10 nm, c) 15 nm, d) 20 nm, and e) 30 nm particles with the wavelength of 1.5418 Å.

As can be seen from Figure 15, as particle size increases, the amplitude of the diffracted peaks increases. The reason is there are a greater number of atoms [in fact, electrons] in bigger nanocrystals, as a result, higher amplitude diffraction peaks occur. In Figure 15.a, the 0^{th} order peak can be seen around $2\theta \approx 5$ degrees. As particle size increases, the amplitudes of the Bragg peaks increase, and the 0^{th} order peaks will be relatively less significant in the diffraction pattern, however they do not completely vanish. In Figure 15a, for the 5 nm particle, the widths of the peaks are so high that peaks overlap with each other at the angles of 41, 79, and 114 degrees. As particle size increases, the breadth of the peaks decreases. Having both enhancements in the Bragg peaks amplitude and decrease in the broadening of the Bragg peaks for the bigger nanocrystals, make them appear as impulse functions. For bulk crystals, these peaks are ideal Dirac delta functions [84], [85].

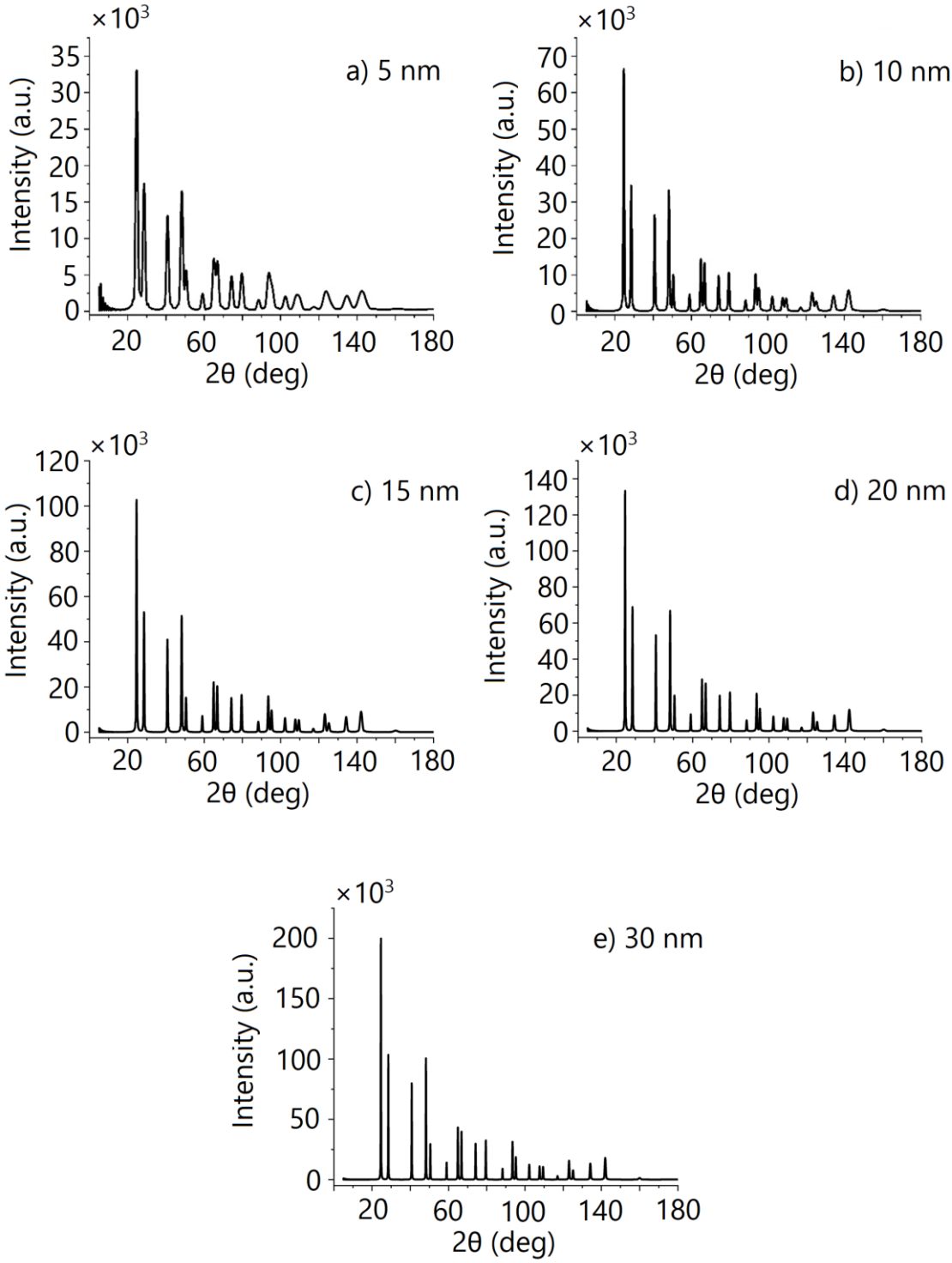

Figure 16 Angular intensity distributions of five energy-minimized spherical gold nanocrystals with different sizes (at 0 K and ambient pressure), a) 5 nm, b) 10 nm, c) 15 nm, d) 20 nm, and e) 30 nm particles with the wavelength of 1.0 Å.

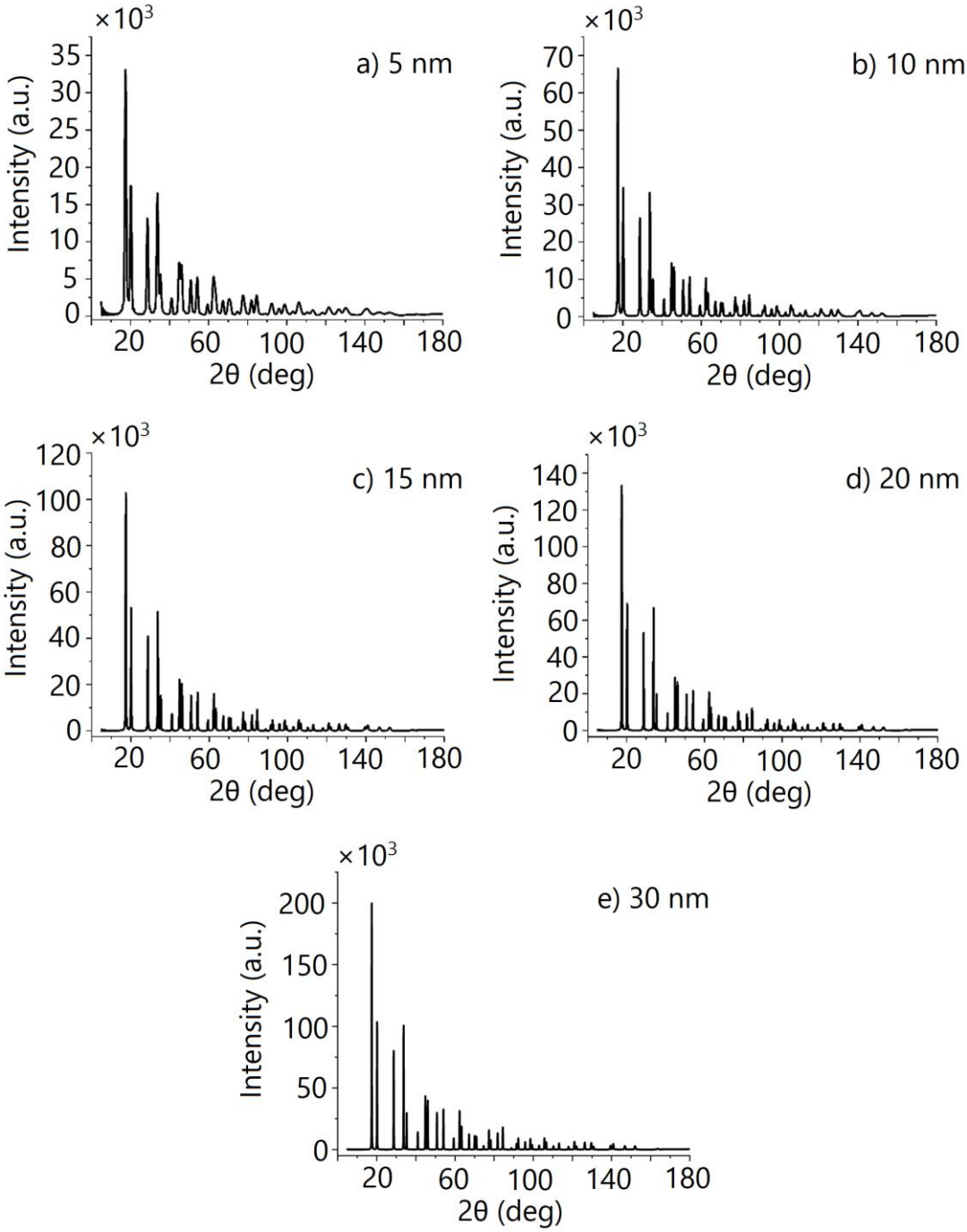

Figure 17 Angular intensity distributions of five energy-minimized spherical gold nanocrystals with different sizes (at 0 K and ambient pressure), a) 5 nm, b) 10 nm, c) 15 nm, d) 20 nm, and e) 30 nm particles with the wavelength of 0.71073 Å.

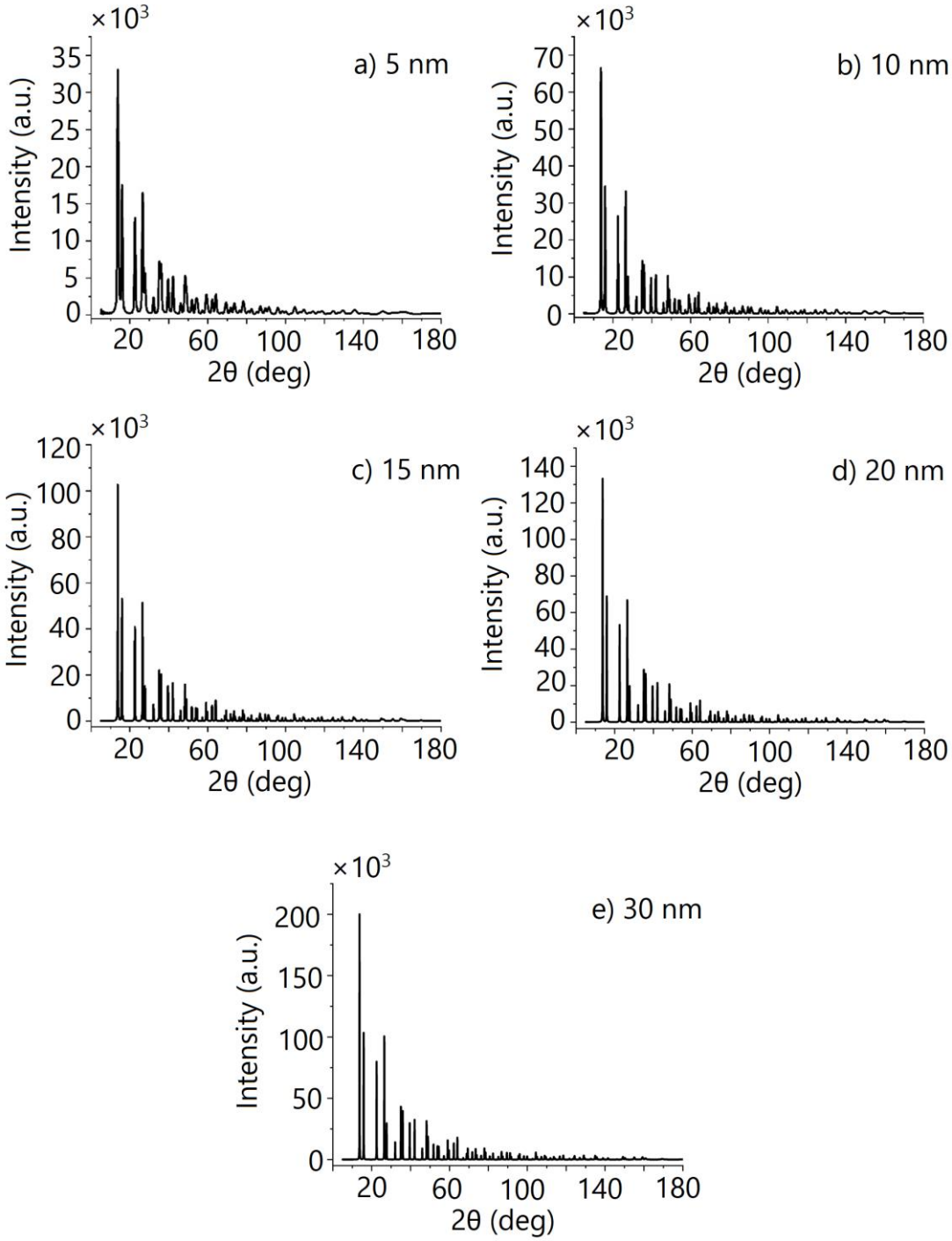

Figure 18 Angular intensity distributions of five energy-minimized spherical gold nanocrystals with different sizes (at 0 K and ambient pressure), a) 5 nm, b) 10 nm, c) 15 nm, d) 20 nm, and e) 30 nm particles with the wavelength of 0.560871 Å.

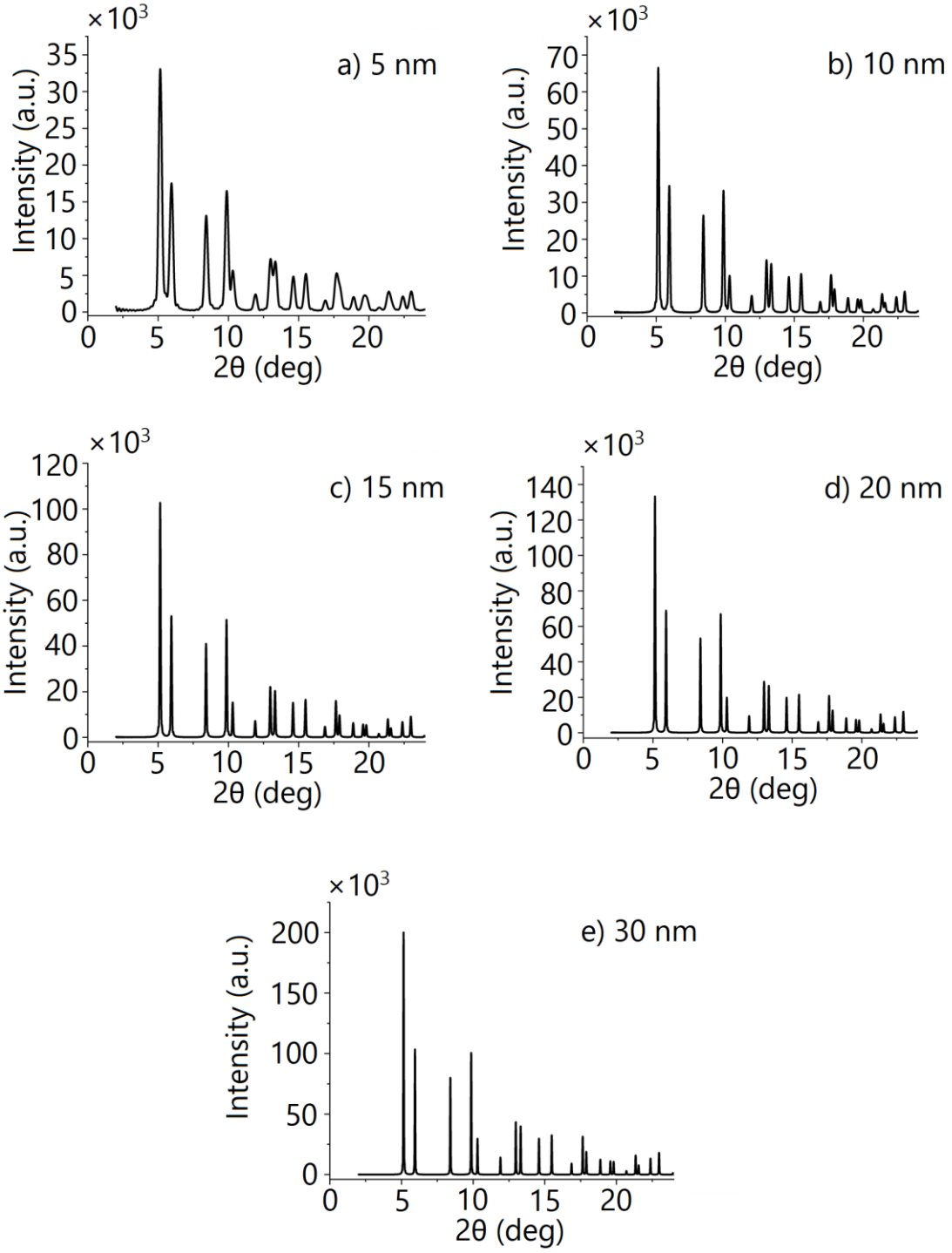

Figure 19 Angular intensity distributions of five energy-minimized spherical gold nanocrystals with different sizes (at 0 K and ambient pressure), a) 5 nm, b) 10 nm, c) 15 nm, d) 20 nm, and e) 30 nm particles with the wavelength of 0.210616 Å in the 2θ range of 2 to 24 degrees. The 2θ range is decreased for a higher resolution over the first peaks.

Figure 19 shows the range of 2θ from 5 to 24 degrees which contains the first 20 peaks. These peaks show the most powerful reflections. From Figure 15 to Figure 19, it can be understood that there are a lot of wavelengths that can be chosen from the existing ones (must be chosen from Kα wavelengths of target metals of the assumed monochromatic X-ray source, i.e., Tungsten, Copper, Zinc, etc.), and none of them are the right or wrong choice. Based on the existing apparatus and problems, any one of the wavelengths can be used. Starting from the highest wavelength of 1.5418 Å (Figure 15) to the smallest wavelength of 0.210616 Å (Figure 19), the peaks shift to the left and they become thinner in width, but there is no change in their intensities as a function of wavelength. It is in accordance with Bragg's equation (Eq. (1)), which shows as the wavelength decreases, the Bragg reflection angles also decrease. As mentioned, when particle size is constant and wavelength varies, intensities do not change in their magnitude, because the number of atoms remains constant. In fact, number of electrons is important, and while the number of atoms is the same, and no electric charge is assumed, the number of electrons also remains constant.

At constant wavelength, as the particle size increases, the intensities increase, and the peak widths decrease comparatively. This is also predicted by the Scherrer equation. It is natural because as particle size increases, nanocrystals become more like bulk crystals. In bulk crystals, the intensity profiles are relatively thinner than the nanocrystals. The bulk intensity peaks look like delta Dirac functions, because there are many electrons making the constructive interference, while in the nanocrystals, both the small number of atoms and large STV atom ratio have roles in increasing the widths for the Bragg peaks.

As seen in Figure 15 to Figure 19, 0^{th} order intensity also shifts to the left, as the wavelength decreases. Lower wavelengths have higher Q_{max} as long as the scattering angle is kept constant. The only drawback is the restrictions in the apparatus. New generation synchrotrons are required for performing high energy diffraction [86], [87].

Bragg's law should always be considered while double-checking the intensities. For instance, Figure 20 shows the diffraction pattern of a 15 nm gold nanocrystal illuminated by 0.71073 Å X-rays, it shows a tail-like shape at the end of its angular range:

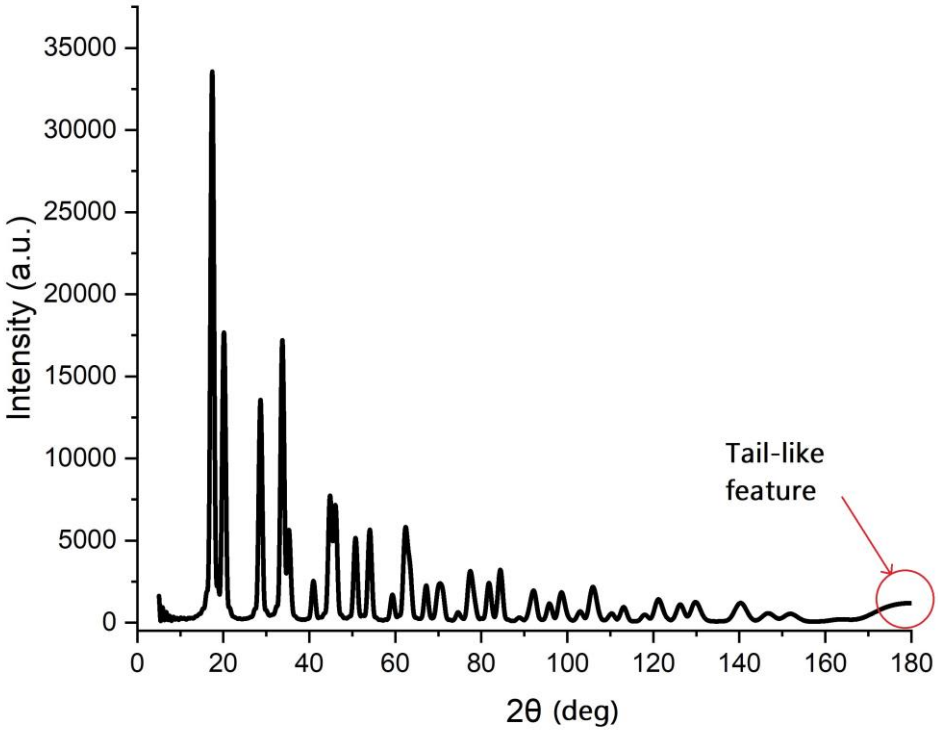

Figure 20 The diffraction pattern of a 15 nm gold nanocrystal with an X-ray of the wavelength 0.71073 Å.

Considering Bragg's law for the suspicious tail-like feature in 2θ ≈ 180 degrees, we have:

$$2dsin(\theta) = \lambda$$

$$d = \frac{\lambda}{2sin(\theta)}$$

$$d = \frac{0.71073}{2sin(90)} = 0.355365 \text{ Å}$$

$$d = \frac{a}{\sqrt{h^2 + k^2 + l^2}}$$

$$0.355365 = \frac{4.07825}{\sqrt{h^2 + k^2 + l^2}}$$

$$\sqrt{h^2 + k^2 + l^2} = 11.4811532$$

$$h^2 + k^2 + l^2 = 131.8168784$$

$$(hkl) \approx (559)$$

As a result, there was a peak at 180 degrees that was cut in half. Peaks should not be cut prematurely when performing PDF analysis, because they contain structural information, and Fourier transforming such diffraction patterns causes inaccuracies in the resulting PDF. Figure 21a shows the PDF refinement of the diffraction pattern in

Figure 20 without the last peak which is cut in half, and Figure 21b illustrates the PDF refinement of the Figure 20 with the tail-like feature.

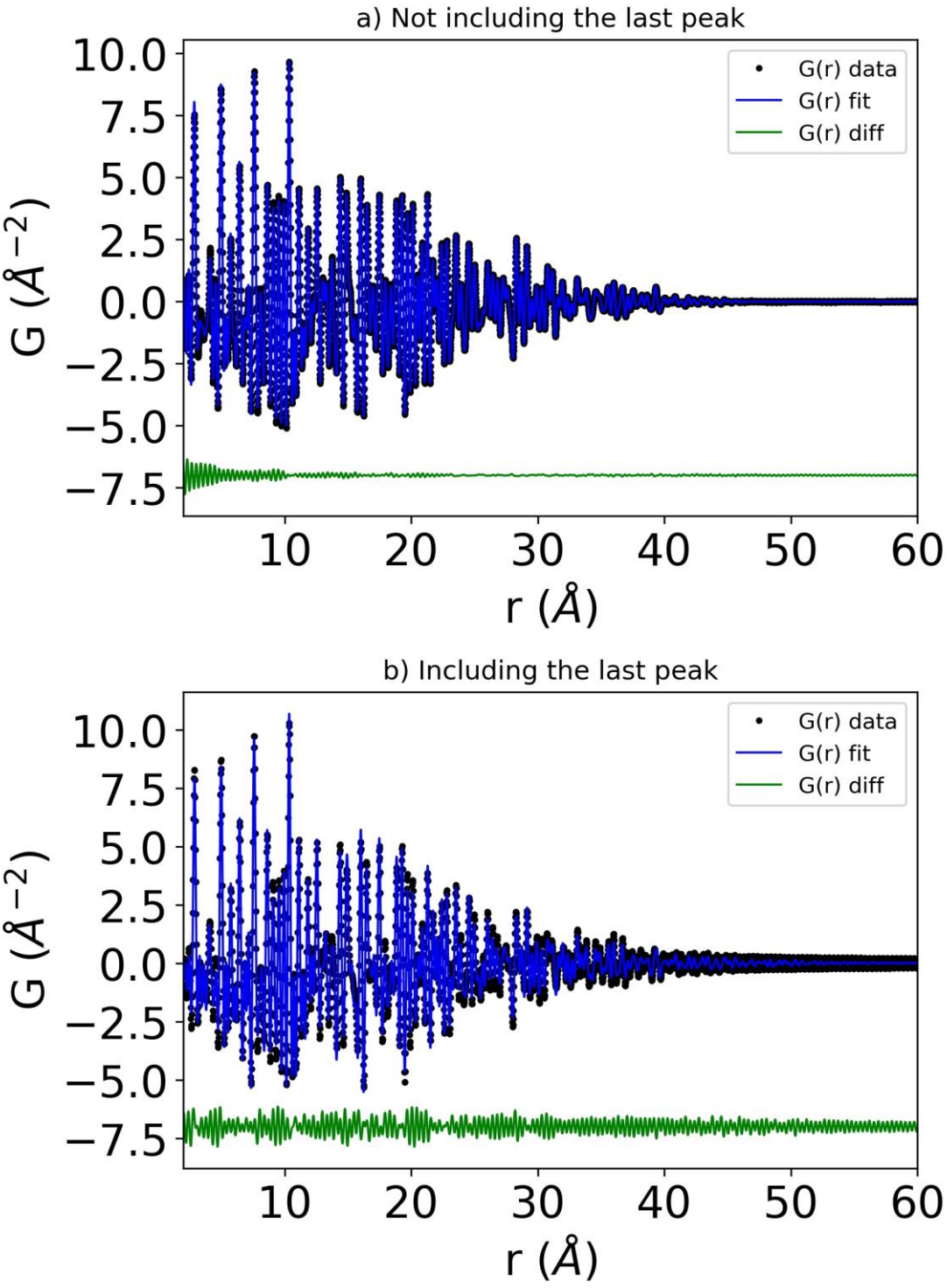

Figure 21 a) PDF results of Figure 20 not including the last halved peak. **b)** PDF results of Figure 20 including the last halved peak. part b shows a higher residual compared to part a.

3.2 Analysis of the extracted parameters

In PDF refinements, initial values for the ADP, lattice parameters, and particle size have been given to start the refinement. The fitting process is made up of three main processes. Step one is fixing all parameters and only letting the scale and lattice parameters to refine. Step two is to fix all the parameters again (including the refined parameters in step one) and refine for particle size. Third step is to fix all the parameters again, and refine for the ADPs. Lattice parameter refinement is important as it has direct impacts on the material properties (e.g. shear stress, strain, etc.) [88]–[90]. Particle size can determine properties like color [91], [92]. ADP is an indicator of the atomic vibrations and possibly the temperature of the samples [93].

3.3 Analysis of crystal size extracted from PDF refinement vs real space calculations

In this section, real space calculations are done on the atomic coordinate file after MD simulations. Also, PDF calculations are shown to see how these methods differ or agree in case of particle size determination. Real space calculations are courtesy of Mr. Merdan Batyrov, PhD student in Ozyegin University.

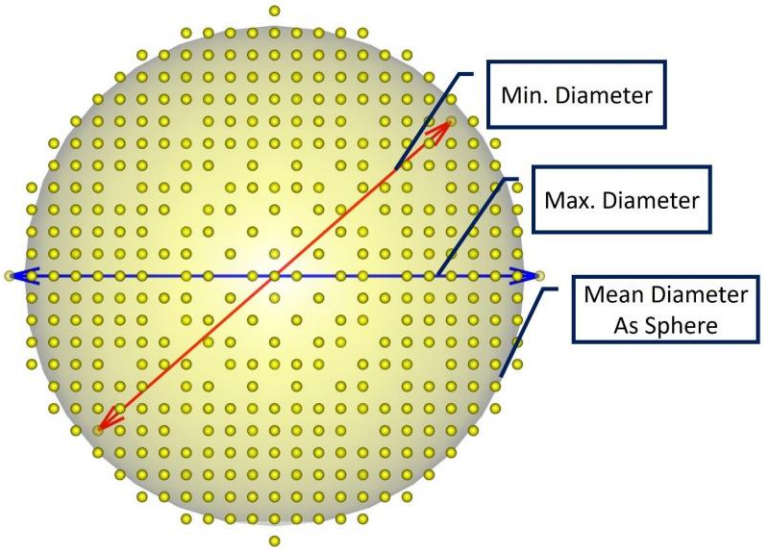

Figure 22 The maximum, minimum, and mean diameter of a spherical gold nanocrystal, using real space calculation. Courtesy of Merdan Batyrov.

Table 2 Distribution of diameters (D) for ideal crystalline particles based on real space calculations.

Nominal Diameter (nm)	*Number of atoms*	*STV atom ratio*	*Max D (Å)*	*Min D (Å)*	*Mean D (Å)*	*Standard deviation (Å)*
5	3589	0.29	48.79	43.42	46.11	1.5
10	28897	0.15	97.53	91.92	94.9	1.5
15	106114	0.10	150.28	144.70	147.74	1.5
20	231477	0.078	195.13	191.05	193.25	1.5
30	781145	0.053	294.19	287.84	292.38	1.4

Table 3 Distribution of diameters (D) for equilibrated crystalline particles (0 K) based on real space calculations.

Nominal Diameter (nm)	*Number of atoms*	*STV atom ratio*	*Max D (Å)*	*Min D (Å)*	*Mean D (Å)*	*Standard deviation (Å)*
5	3589	0.29	48.23	43.43	45.89	1.4
10	28897	0.15	96.93	91.96	94.70	1.3
15	106114	0.10	149.87	144.82	147.59	1.4
20	231477	0.078	194.53	189.42	192.24	1.4
30	781145	0.053	292.05	286.95	289.73	1.4

The results from PDF refinement show the following particle sizes:

Table 4 Diameters (D) for ideal crystalline particles, λ=1.5418 Å based on PDF refinement.

Nominal Diameter (nm)	*Number of atoms*	*STV atom ratio*	*Particle size (Å)*
5	3589	0.29	48.98
10	28897	0.15	97.83
15	106114	0.10	150.79
20	231477	0.078	195.67
30	781145	0.053	294.17

Table 5 Diameters (D) for equilibrated crystalline particles (0 K), λ=1.5418 Å based on PDF refinement.

Nominal Diameter (nm)	*Number of atoms*	*STV atom ratio*	*Particle size (Å)*
5	3589	0.29	47.72
10	28897	0.15	96.39
15	106114	0.10	149.48
20	231477	0.078	194.53
30	781145	0.053	293.08

Figure 22 demonstrates different size parameters for the nanocrystals based on real space calculations and coordination numbers of atoms inside the nanocrystal. Wherever the CN is not equal to 12 for gold nanocrystalline, it means the atoms are at the surface of the particle. The distance between all symmetrically opposite atoms is taken, their minimum, maximum, and mean is reported. Table 4 and Table 5 are obtained from X-ray diffraction and PDF with the wavelength of 1.54 Å, while Table 2 and Table 3 are obtained from real space analysis of data, meaning that all calculations here are based on atomic coordinates directly. Table 2 and Table 3 are obtained by direct statistical analysis of the inputs, that is why they must be stated with minimum, maximum, mean and standard deviation, while for Table 4 and Table 5, this is not the case, and Diffpy would obtain the size based on where the PDF peaks relatively attenuate using LM methods. The reason for choosing the word “relatively” is that there is almost always a small amount of inevitable fluctuation in the PDF that is related to the Fourier transform and has an adverse effect on the exact refined parameters. The

following tables show the particle size for other wavelengths. They present more or less the same results. This shows that particle size in PDF analysis can be obtained regardless of the X-ray wavelength. The reason is that higher energy waves have lower wavelength, which leads to a higher Q_{max} helping to better distinguish the peaks by decreasing their width and increasing their amplitudes.

Table 6 Diameters (D) for ideal crystalline particles, λ=1.0 Å based on PDF refinement.

Nominal Diameter (nm)	*Number of atoms*	*STV atom ratio*	*Particle size (Å)*
5	3589	0.29	48.82
10	28897	0.15	97.76
15	106114	0.10	150.79
20	231477	0.078	195.62
30	781145	0.053	294.07

Table 7 Diameters (D) for equilibrated crystalline particles (0 K), λ=1.0 Å based on PDF refinement.

Nominal Diameter (nm)	*Number of atoms*	*STV atom ratio*	*Particle size (Å)*
5	3589	0.29	46.82
10	28897	0.15	95.33
15	106114	0.10	148.44
20	231477	0.078	193.58
30	781145	0.053	292.15

Table 8 Diameters (D) for ideal crystalline particles, λ=0.71073 Å based on PDF refinement.

Nominal Diameter (nm)	*Number of atoms*	*STV atom ratio*	*Particle size (Å)*
5	3589	0.29	49.07
10	28897	0.15	97.78
15	106114	0.10	150.88
20	231477	0.078	195.68
30	781145	0.053	294.01

Table 9 Diameters (D) for equilibrated crystalline particles (0 K), λ=0.71073 Å based on PDF refinement.

Nominal Diameter (nm)	*Number of atoms*	*STV atom ratio*	*Particle size (Å)*
5	3589	0.29	45.97
10	28897	0.15	94.51
15	106114	0.10	147.47
20	231477	0.078	192.69
30	781145	0.053	291.16

Table 10 Diameters (D) for ideal crystalline particles, λ=0.560871 Å based on PDF

refinement.

Nominal Diameter (nm)	*Number of atoms*	*STV atom ratio*	*Particle size (Å)*
5	3589	0.29	48.80
10	28897	0.15	97.46
15	106114	0.10	150.54
20	231477	0.078	195.30
30	781145	0.053	293.51

Table 11 Diameters (D) for equilibrated crystalline particles (0 K), λ=0.560871 Å based on PDF refinement.

Nominal Diameter (nm)	*Number of atoms*	*STV atom ratio*	*Particle size (Å)*
5	3589	0.29	44.85
10	28897	0.15	93.72
15	106114	0.10	146.38
20	231477	0.078	191.56
30	781145	0.053	289.86

Table 12 Diameters (D) for ideal crystalline particles, λ=0.210616 Å based on PDF refinement.

Nominal Diameter (nm)	*Number of atoms*	*STV atom ratio*	*Particle size (Å)*
5	3589	0.29	48.74
10	28897	0.15	97.64
15	106114	0.10	150.55
20	231477	0.078	195.45
30	781145	0.053	293.97

Table 13 Diameters (D) for equilibrated crystalline particles (0 K), λ=0.210616 Å based on PDF refinement.

Nominal Diameter	*Number of atoms*	*STV atom ratio*	*Particle size (Å)*
5	3589	0.29	44.20
10	28897	0.15	93.48
15	106114	0.10	145.91
20	231477	0.078	191.01
30	781145	0.053	289.61

Table 4 to Table 13 show slight changes. This means accuracy of the particle size determination does not change much as the wavelength changes. As the wavelength decreases, the particle size of the energy-minimized samples also decreases. However, for the ideal nanocrystals they give constant results.

Taking the mean of diameters from real space calculations, for the ideal nanocrystals, real space calculations show slightly smaller diameters (Table 2, Table 4, Table 6, Table 8, Table 10, and Table 12). For equilibrated samples, in PDF results, as wavelength decreases, the calculated particle size decreases. The average of these particles for all the wavelengths is almost equal to the mean diameter resulting from real space calculations. For instance, the nominal 5 nm particle has a real space diameter mean of 46.1 Å, averaging over the five wavelengths of PDF results in a diameter of 45.9 Å.

3.4 Analysis of Atomic Displacement Factor Extracted from PDF refinements

As there are five different wavelengths and five different particle sizes, PDF calculations for ideal and refined nanocrystals give following results:

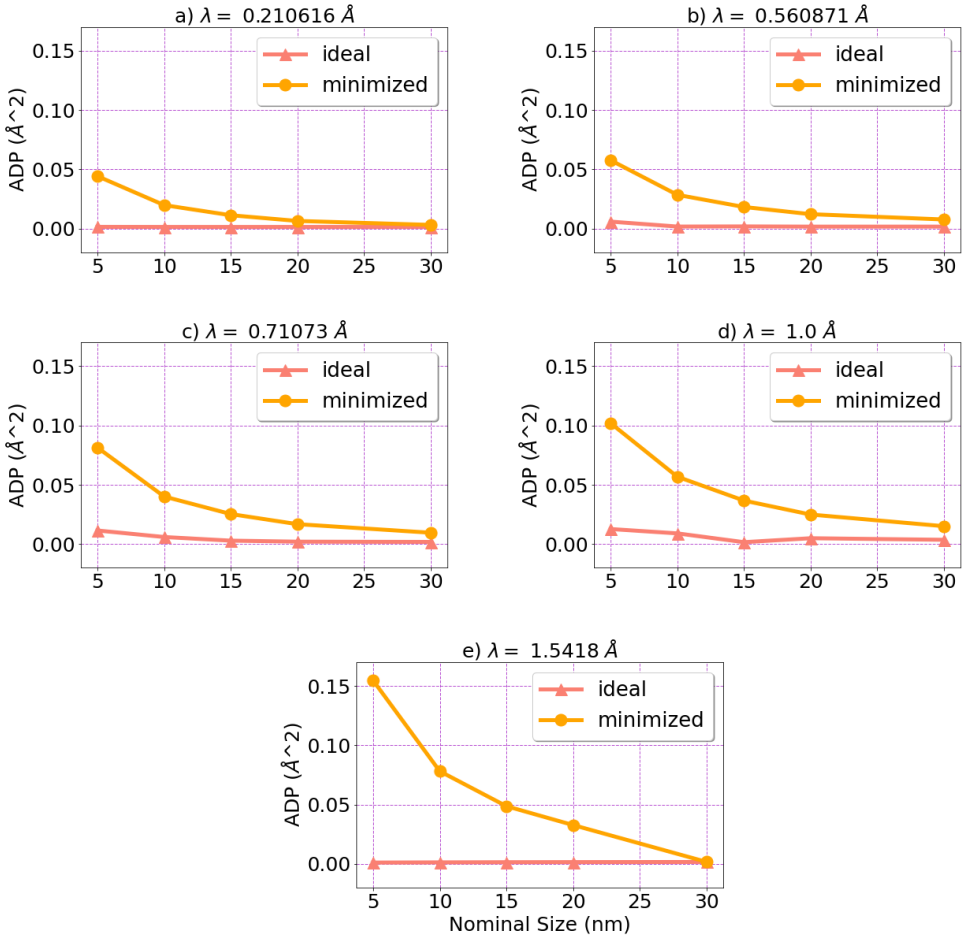

Figure 23 ADP of different particle sizes. Ideal particles are in ideal ambient conditions, and energy-minimized ones are in MD energy-minimized conditions at 0 K temperature and ambient pressure.

Figure 23 shows ADP vs. Particle sizes for both ideal and MD energy-minimized nanocrystals at ambient pressure and 0 K temperature. In ideal nanocrystals, ADP is independent from the particle size, but in energy-minimized counterparts, as particle size increases, the ADP values of the energy-minimized and ideal nanocrystals get closer to each other. It means, as nanocrystalline size decreases, the ADPs increase. Figure 23 also shows that for shorter wavelengths (or higher energy waves), the ADP values of the smaller nanocrystals have less difference (between ideal and energy-minimized particles) than the higher wavelengths. However, for larger nanocrystals (e.g., 30 nm), the ADP's do not differ very much from their theoretical amounts.

3.5 Analysis of Lattice Parameters Extracted from PDF refinements

Figure 24 illustrates the extracted lattice parameters from PDF refinements performed on simulated diffraction data of gold nanoparticle ensembles irradiated by 5 different X-ray wavelengths. It shows as the energy-minimized nanocrystalline size decreases, the lattice parameter also decreases. The y-axis of Figure 24 is illustrated as a/a_0, where a_0 is the lattice parameter read from the CIF file, which has the value of 4.07825 Å.

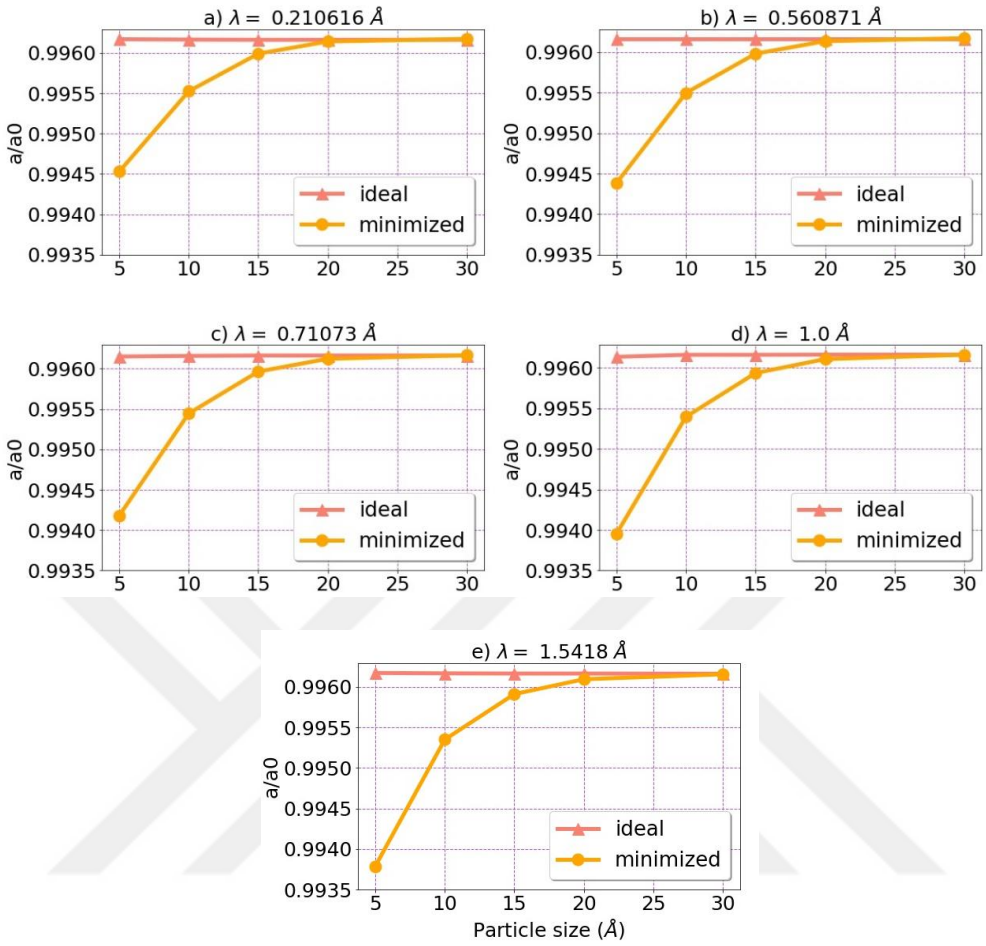

Figure 24 Lattice parameters extracted from PDF refinement performed on simulated diffraction data of gold nanoparticle ensembles irradiated by 5 different wavelengths of X-rays. a_0 is read from the CIF file, and its value is 4.07825 Å.

3.6 Analysis of Peak Widths Extracted from PDF refinements

Considering the width of the first six peaks observed in Figure 13, the following is depicted for 5 nm, 10 nm, and 15 nm, 20 nm, and 30 nm ideal and energy-minimized nanocrystals:

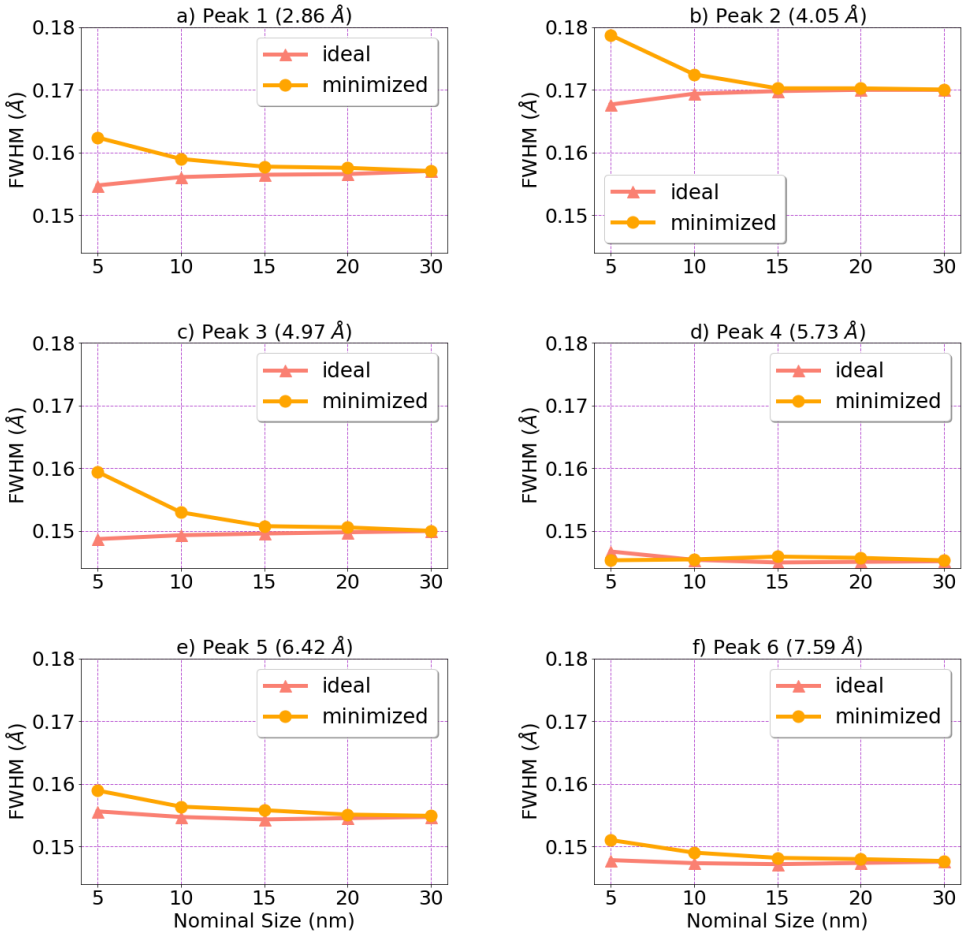

Figure 25 FWHM's for the first six peaks, both for ideal and energy-minimized nanocrystals with an X-ray wavelength of λ = 0.71073 Å. Particle sizes are 5 nm, 10 nm, 15 nm, 20 nm, and 30 nm.

Figure 25, illustrates the FWHM of the ideal and nanocrystals as a function of the particle sizes. FWHM of the peaks is obtained by performing a Gaussian fit to the peaks all together. This analysis was done on the ideal and energy-minimized 5 nm, 10 nm, 15 nm, 20 nm, and 30 nm nanocrystals with the X-ray wavelength of $\lambda = 0.71073$ Å. Width of each peak for each particle size was taken and illustrated in Figure 25. All the subplots agree that, as the particle size increases, the difference between ideal and energy-minimized FWHM decreases, and the maximum difference is for the smallest nanocrystals. These results state that for the very small nanoparticles (e.g., 5 nm), the peak breadth of the energy-minimized nanocrystals is wider than the ideal counterparts. Energy-minimized samples have nonzero ADP amounts, while the ADP of the ideal samples is zero. Therefore, there are atomic displacements in the energy-minimized nanocrystals which will lead to broader peaks compared to ideal nanocrystals. Also, 5 nm nanocrystals, compared to 10 nm nanocrystals, have higher value of STV atom ratio. That is why the breadth of the peaks decrease as the nanocrystals increase in size.

3.7 Dependency of the refinement quality on Q_{damp}

The results of the simulations with different Q_{damp} values have shown a high dependency on Q_{damp}. This value is a damping parameter and needs to be set experimentally. As already mentioned, the usual values for Q_{damp} are between 0.02 to 0.04 [80]–[82]. However, some sources [94] stated that because of the high resolution of the 2θ, the values might even decrease to less than 0.001 for Q_{damp}. For obtaining a reliable Q_{damp}, we need to do a sensitivity test on our data. To understand the best possible amount of Q_{damp}, different values have been given to the program and

refinements were done based on them. The following is the result of different Q_{damp} values versus four different parameters: Residual, particle size, lattice parameter and ADP. For a higher calculation speed, the ideal 5 nm particle is under observation. Figure 31 to Figure 40 show the PDF refinement results for the wavelength of $\lambda = 0.21$ Å, because of the high Q_{max} and energy of the wave.

Comparing the true particle size for Figure 26, which is 48.875 Å, it can be understood that the minimum possible Q_{damp} is the best option for this analysis. Figure 27 to Figure 40 also support this conclusion. For this observation, a range of possible Q_{damp} amounts, (0.001, 0.02) is given, but the results showed this range is not proper because it makes scattered false results. In the second study, the range was reduced to (0.001, 0.01) and the results are as the following figures:

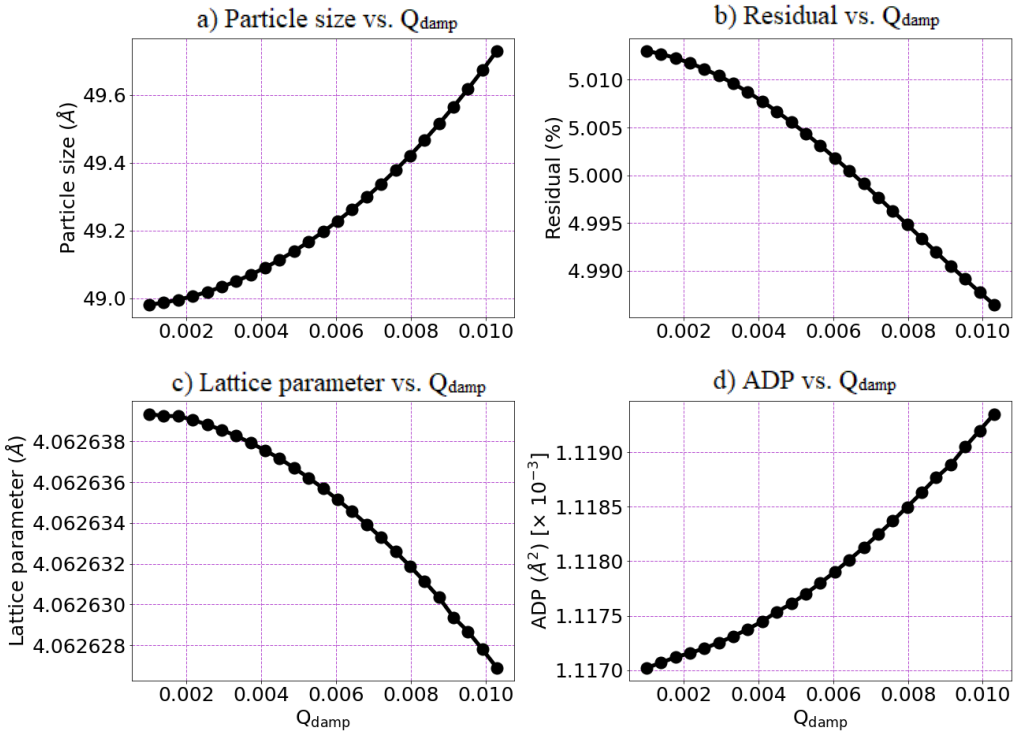

Figure 26 Q_{damp} range of (0.001, 0.01), **a)** Particle size, **b)** Residual, **c)** Lattice parameter, and **d)** ADP vs. Q_{damp} for λ=1.54 Å and the ideal 5 nm particle.

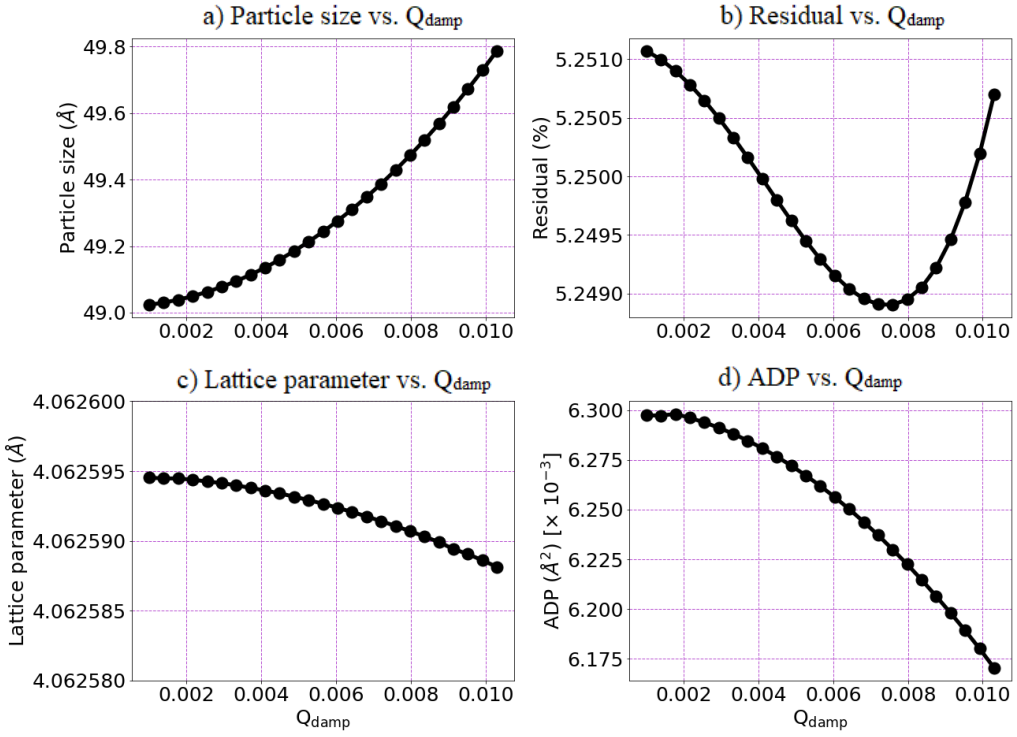

Figure 27 Q_{damp} range of (0.001, 0.01), **a)** Particle size, **b)** Residual, **c)** Lattice parameter, and **d)** ADP vs. Q_{damp} for λ=1.0 Å and the ideal 5 nm particle.

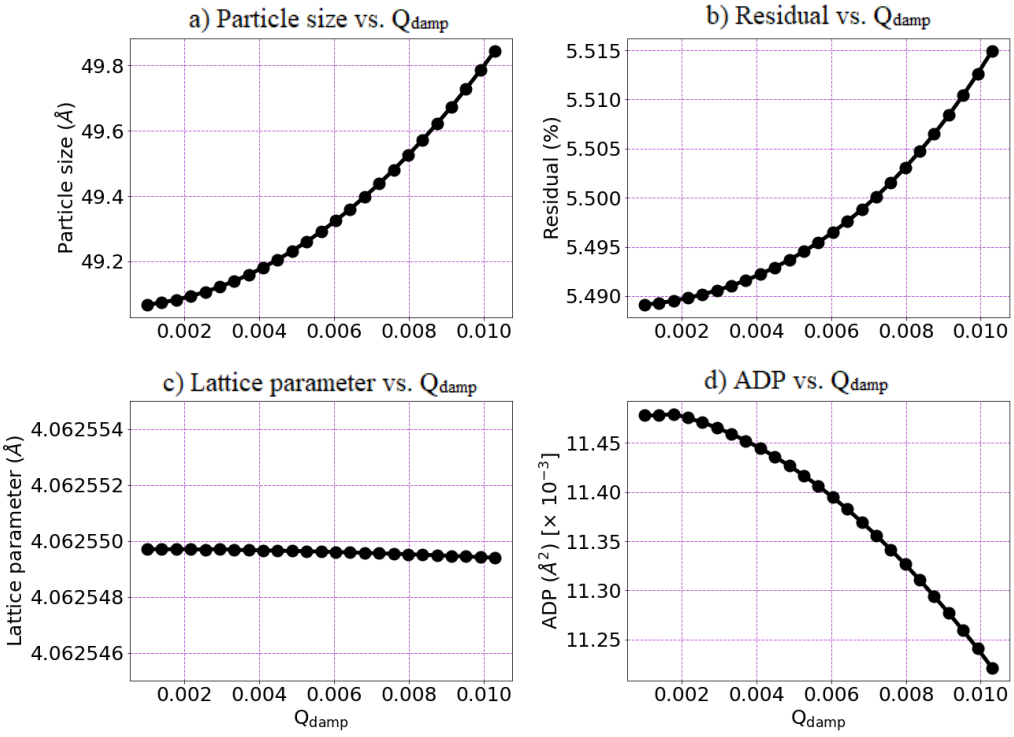

Figure 28 Q_{damp} range of (0.001, 0.01), **a)** Particle size, **b)** Residual, **c)** Lattice parameter, and **d)** ADP vs. Q_{damp} for λ=0.71 Å and the ideal 5 nm particle.

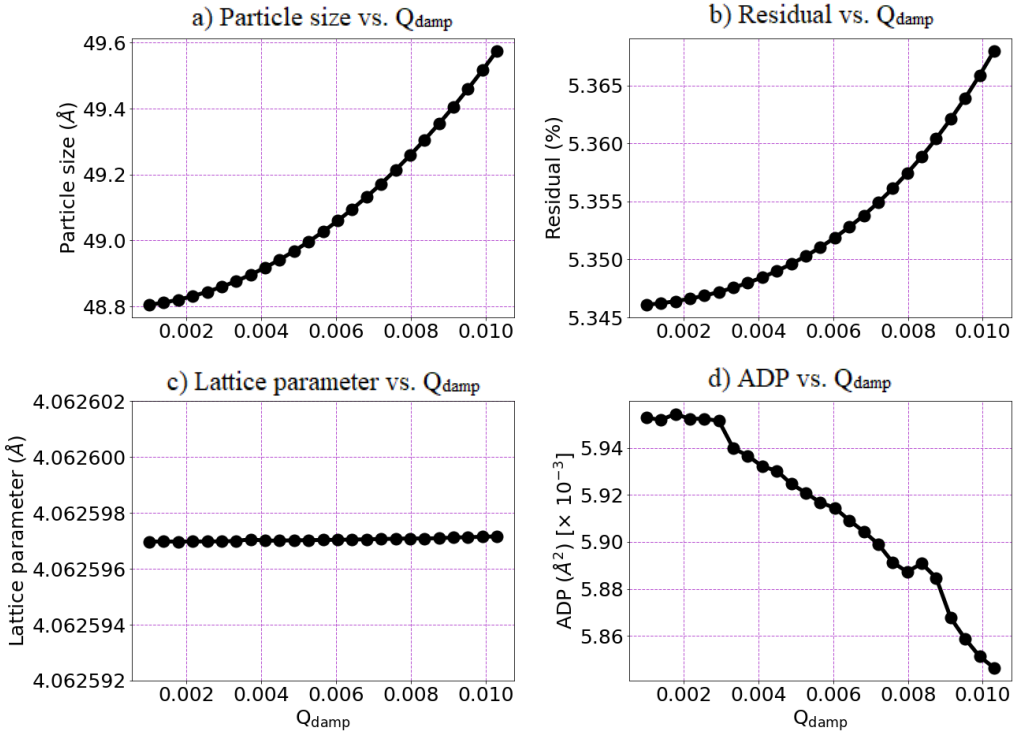

Figure 29 Q_{damp} range of (0.001, 0.01), **a)** Particle size, **b)** Residual, **c)** Lattice parameter, and **d)** ADP vs. Q_{damp} for λ=0.56 Å and the ideal 5 nm particle.

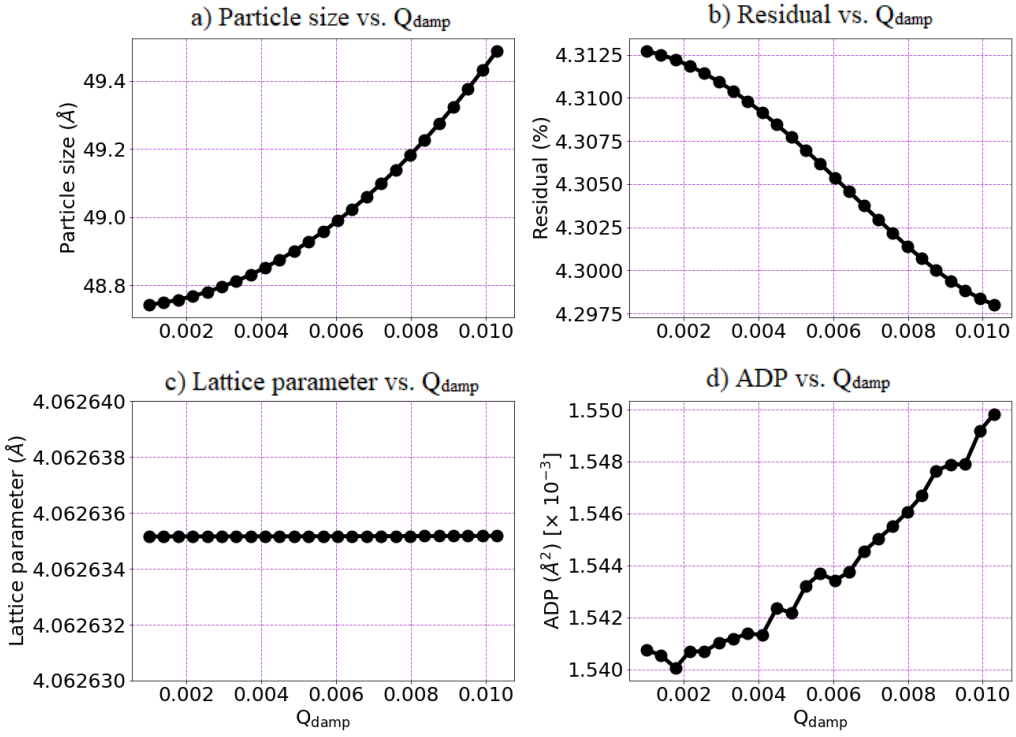

Figure 30 Q_{damp} range of (0.001-0.01), **a)** Particle size, **b)** Residual, **c)** Lattice parameter, and **d)** ADP vs. Q_{damp} for λ=0.21 Å and the ideal 5 nm particle.

Above figures show the dependence of refined parameters on Q_{damp}. The results show the direct impact of Q_{damp} on the residual, particle size, and ADP, but it almost has no effect on the lattice parameter, meaning lattice parameter is almost constant at any Q_{damp} value. As a result, setting the value of Q_{damp} appropriately is an important factor for obtaining the true values of ADP, and particle size. A more detailed observation could be made by restricting the ranges of Q_{damp} between (0.001-0.003). The reason for selecting this range of Q_{damp} is the very small change in the residual, which is less than %1, and it can be a good criterion for understanding which range of Q_{damp} is safe. Considering only one wavelength, the results for the different particle sizes are as follows (λ=0.71 Å):

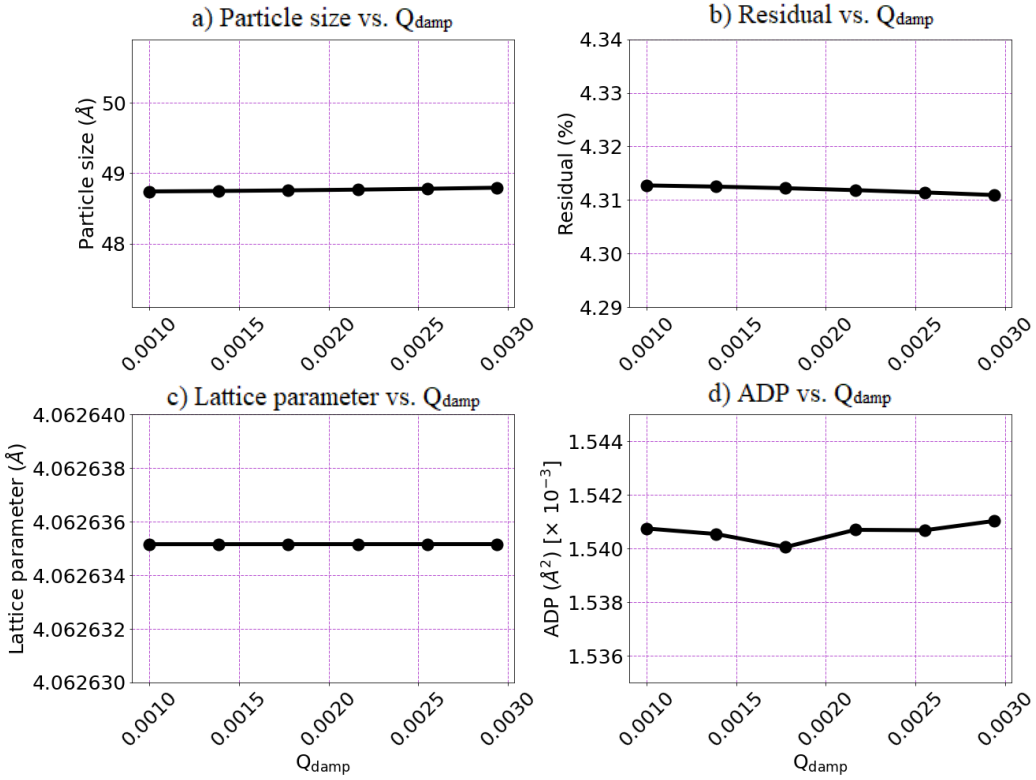

Figure 31 Q_{damp} range of (0.001, 0.003), **a)** Particle size, **b)** Residual, **c)** Lattice parameter, and **d)** ADP vs. Q_{damp} for λ=0.21 Å and the ideal 5 nm particle.

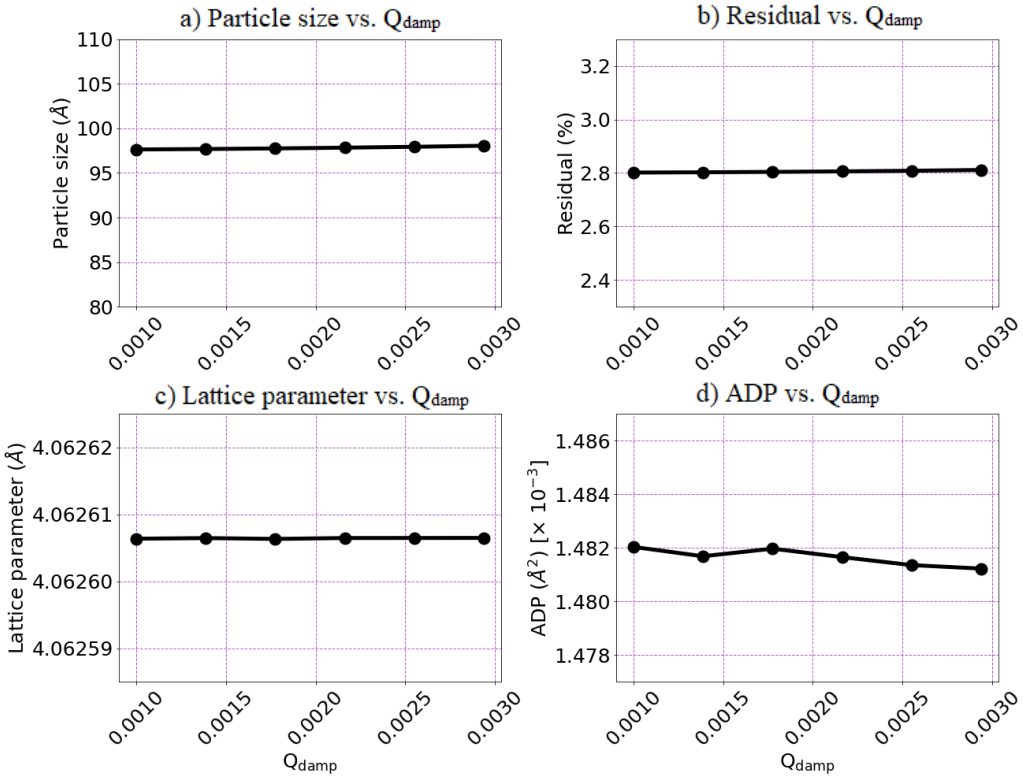

Figure 32 Q_{damp} range of (0.001, 0.003), **a)** Particle size, **b)** Residual, **c)** Lattice parameter, and **d)** ADP vs. Q_{damp} for λ=0.21 Å and the ideal 10 nm particle.

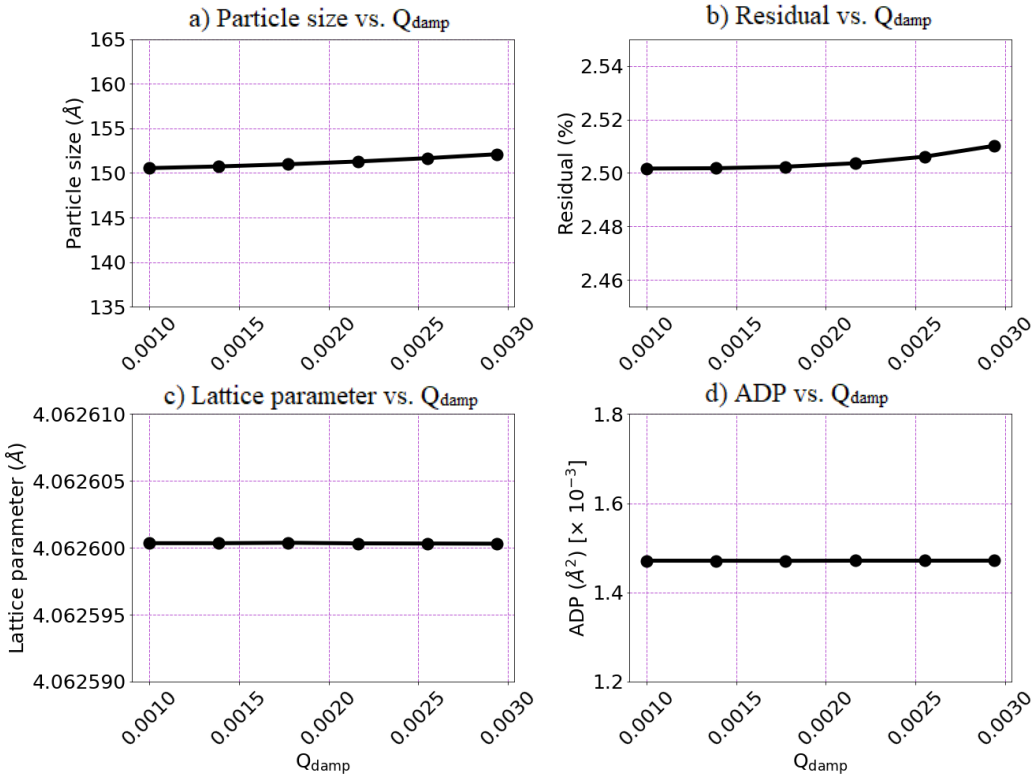

Figure 33 Q_{damp} range of (0.001, 0.003), **a)** Particle size, **b)** Residual, **c)** Lattice parameter, and **d)** ADP vs. Q_{damp} for λ=0.21 Å and the ideal 15 nm particle.

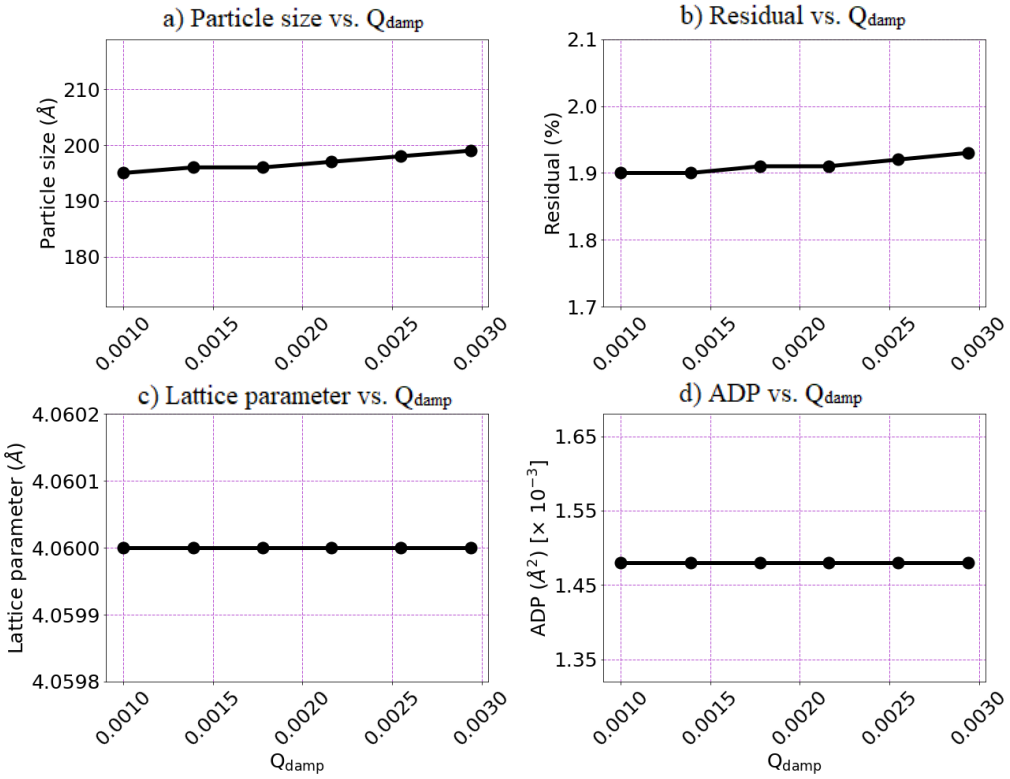

Figure 34 Q_{damp} range of (0.001, 0.003), **a)** Particle size, **b)** Residual, **c)** Lattice parameter, and **d)** ADP vs. Q_{damp} for λ=0.21 Å and the ideal 20 nm particle.

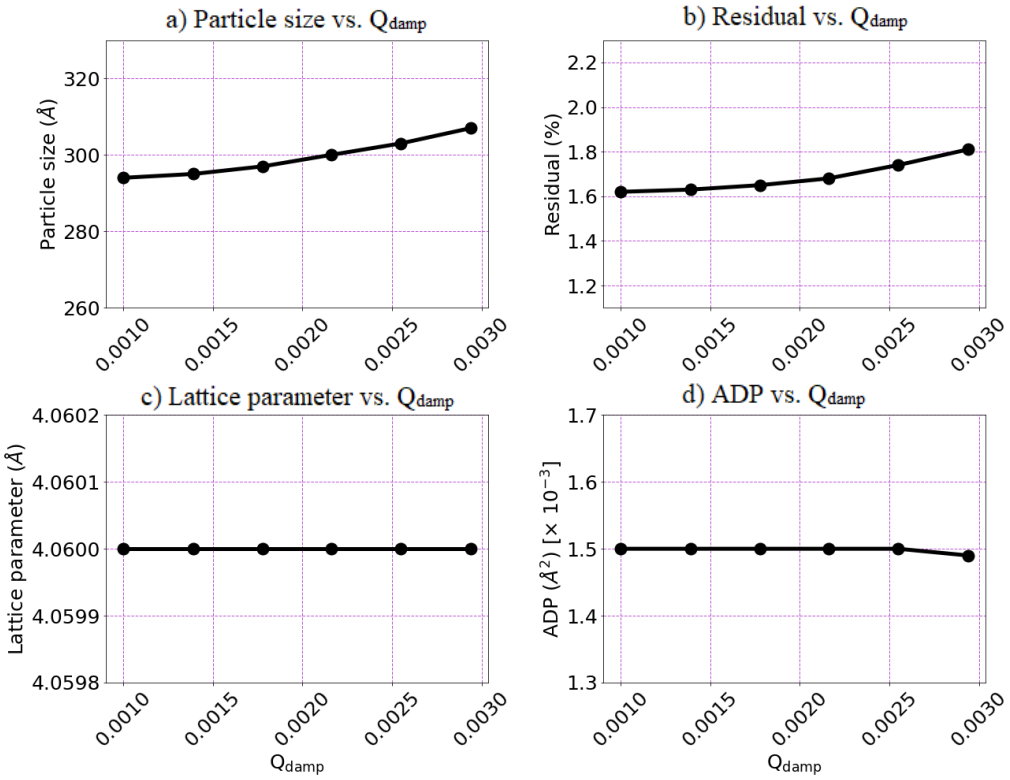

Figure 35 Q_{damp} range of (0.001, 0.003), **a)** Particle size, **b)** Residual, **c)** Lattice parameter, and **d)** ADP vs. Q_{damp} for λ=0.21 Å and the ideal 30 nm particle.

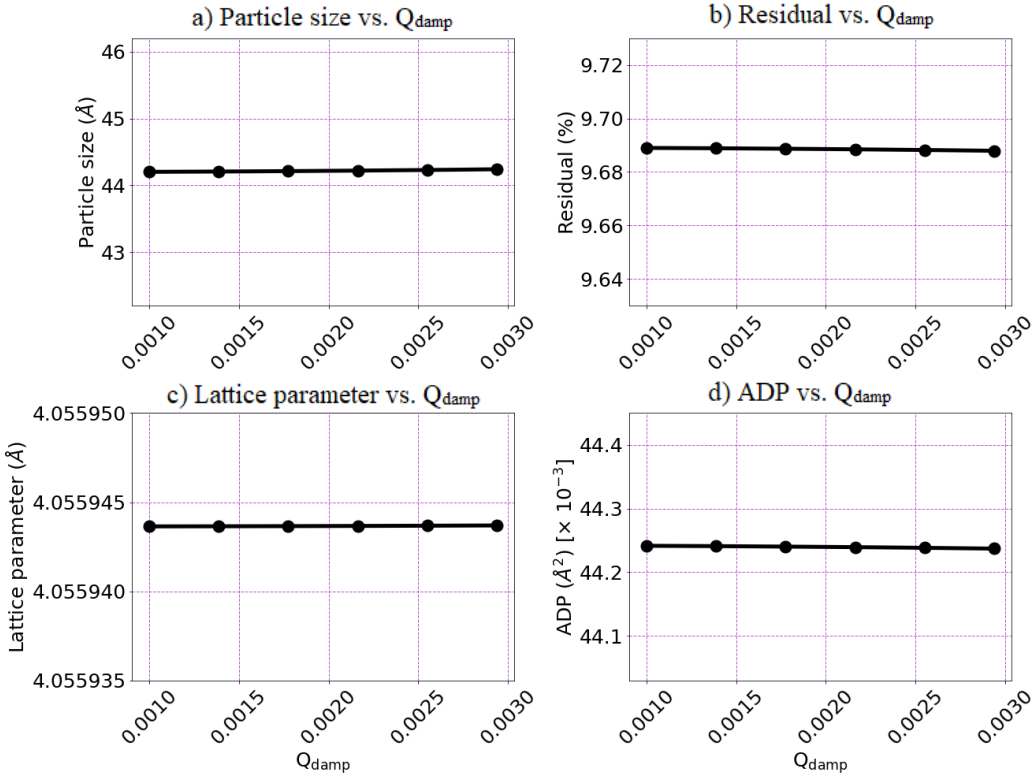

Figure 36 Q_{damp} range of (0.001, 0.003), **a)** Particle size, **b)** Residual, **c)** Lattice parameter, and **d)** ADP vs. Q_{damp} for λ=0.21 Å and the energy-minimized 5 nm particle.

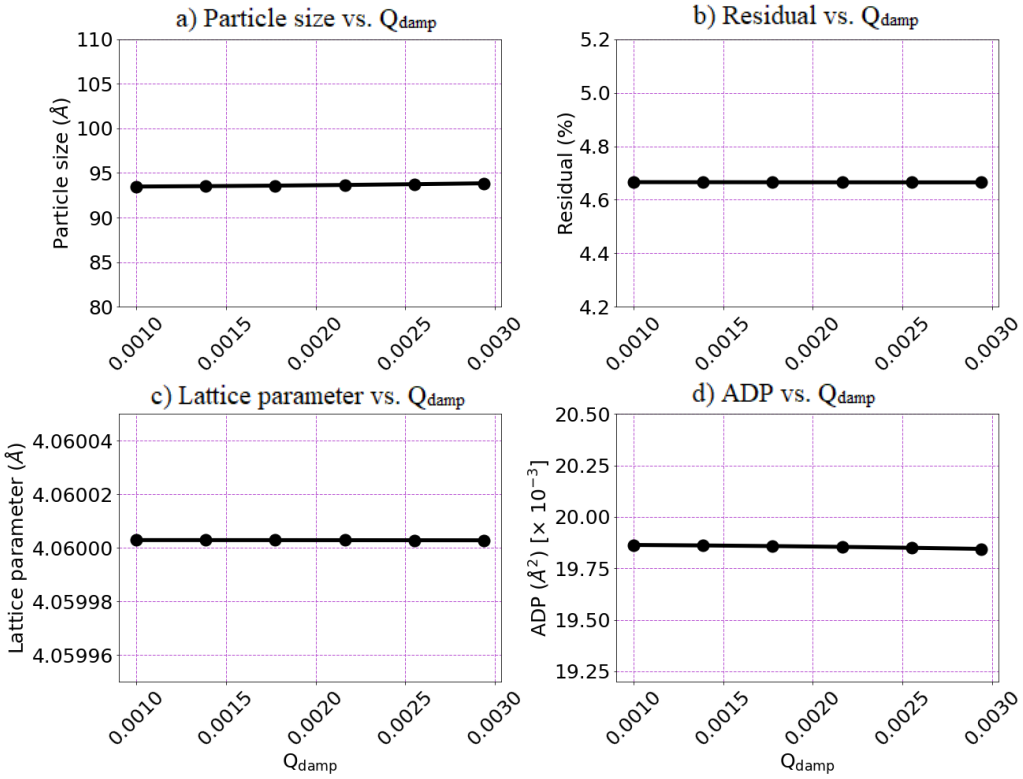

Figure 37 Q_{damp} range of (0.001, 0.003), **a)** Particle size, **b)** Residual, **c)** Lattice parameter, and **d)** ADP vs. Q_{damp} for λ=0.21 Å and the energy-minimized 10 nm particle.

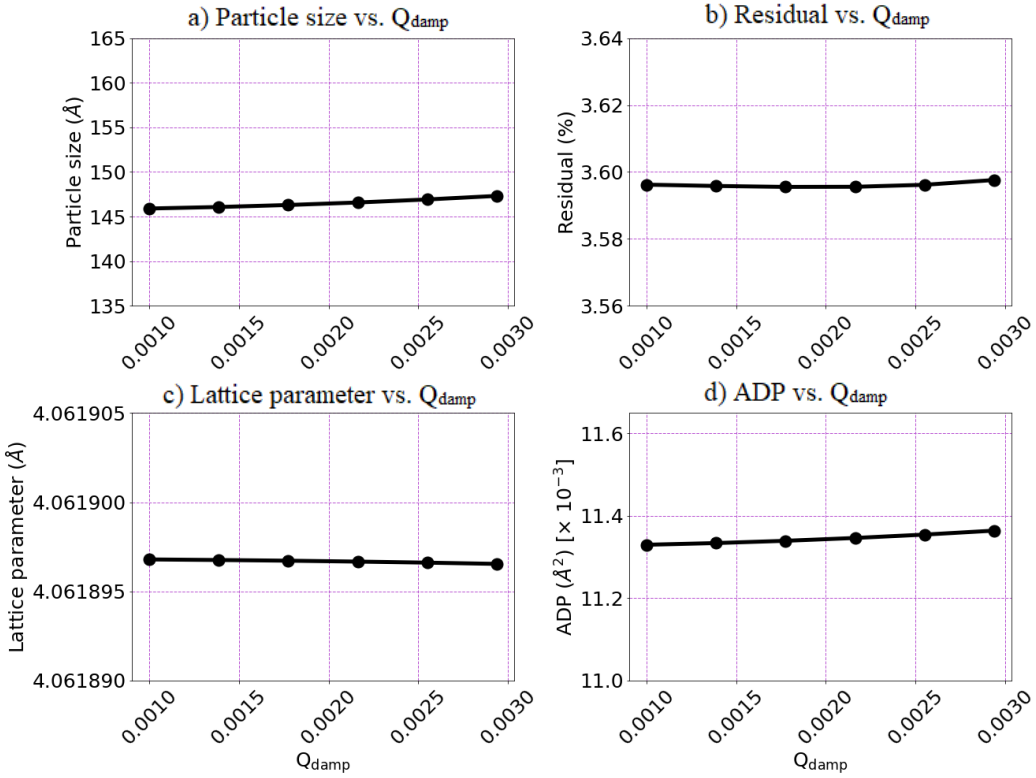

Figure 38 Q_{damp} range of (0.001, 0.003), **a)** Particle size, **b)** Residual, **c)** Lattice parameter, and **d)** ADP vs. Q_{damp} for λ=0.21 Å and the energy-minimized 15 nm particle.

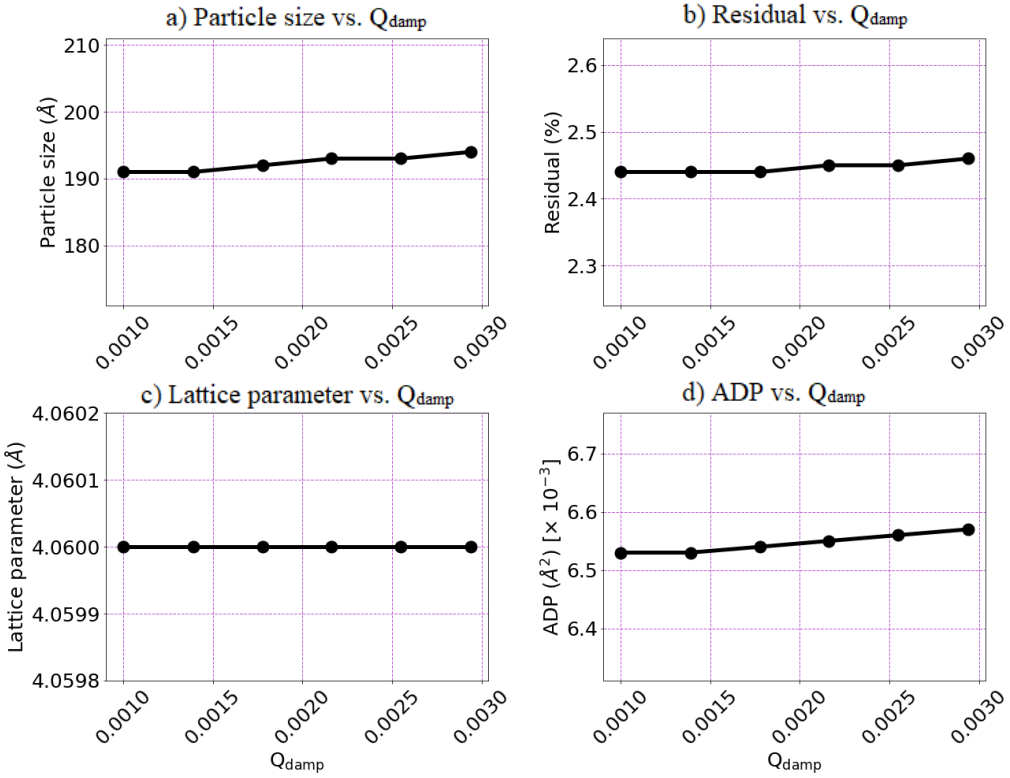

Figure 39 Q_{damp} range of (0.001, 0.003), **a)** Particle size, **b)** Residual, **c)** Lattice parameter, and **d)** ADP vs. Q_{damp} for λ=0.21 Å and the energy-minimized 20 nm particle.

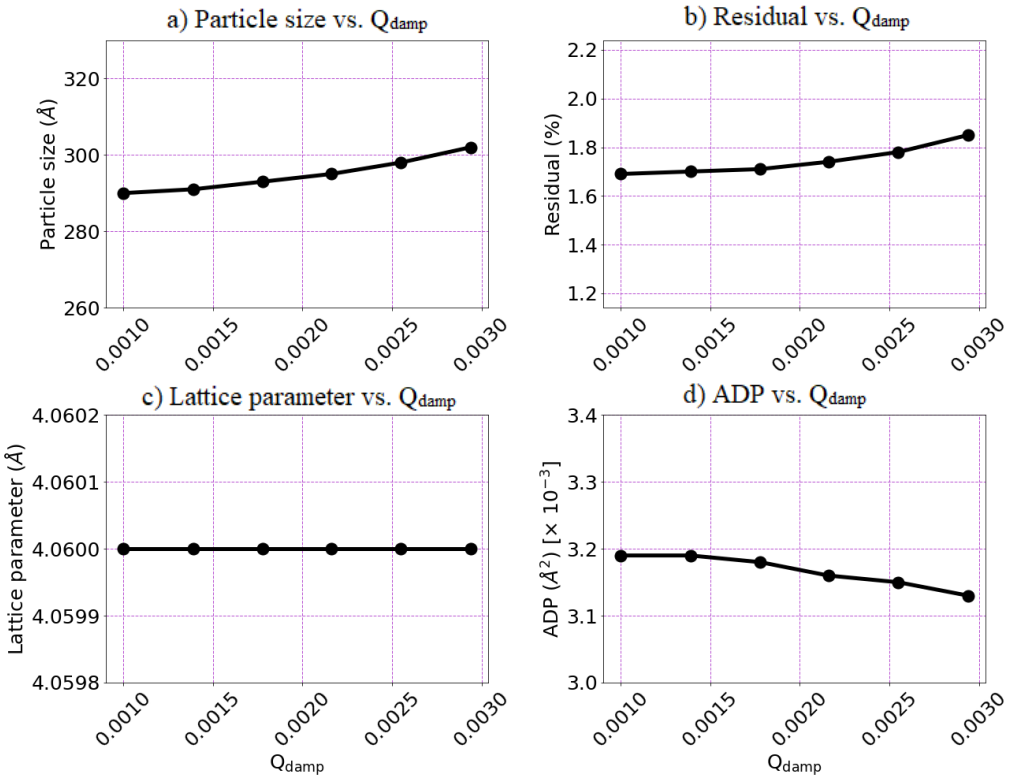

Figure 40 Q_{damp} range of (0.001, 0.003), **a)** Particle size, **b)** Residual, **c)** Lattice parameter, and **d)** ADP vs. Q_{damp} for λ=0.21 Å and the energy-minimized 30 nm particle.

Figure 26 to Figure 40 show a constant change (increase or decrease) in the results which grows continuously. As a result, the range of Q_{damp} should be the amounts that yield the best results. As can be seen in the results above, the best possible amount for Q_{damp} is the minimum of them, which is 0.001, because the parameters obtained while Q_{damp}=0.001 is the closest to the real (predicted) values of the parameters. That is why in all the simulations, Q_{damp} is taken as 0.001 and as it is not set as a refinable parameter, there is no other complexity or relations between Q_{damp} and other parameters. However, other parameters like lattice parameter, particle size, ADP, etc. should be chosen with great care as they are getting refined. These parameters are in direct

relation with each other. The refinement and initial value of one, has a direct impact on the total process of refinement and the last refinement.

The above results were obtained by dividing the Q_{damp} range of (0.001, 0.02) to 50 equally spaced parts and doing the total refinements using each of these 50 amounts one by one. Each time the Q_{damp} changes, the refinements start from the beginning.

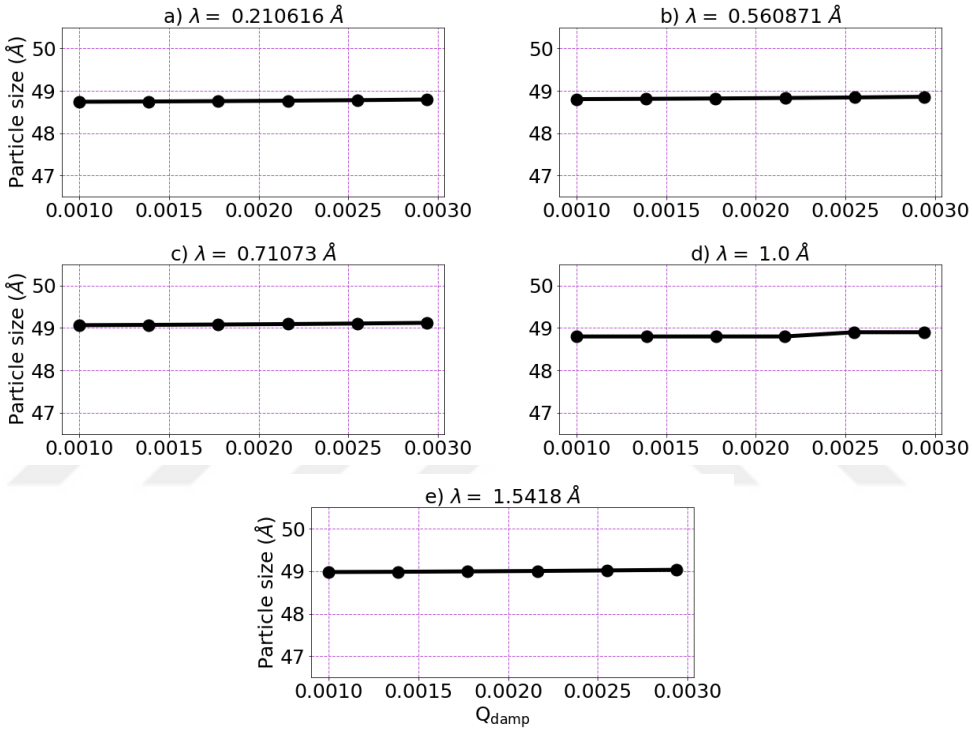

Figure 41 Q_{damp} range of (0.001, 0.003) vs. particle size for **a)** λ=0.21 Å, **b)** λ=0.56 Å, **c)** λ=0.71 Å, **d)** λ=1.0 Å, and **e)** λ=1.54 Å, respectively. The illuminated sample is ideal 5 nm particle (The exact particle size is 48.75).

Figure 41 illustrates Q_{damp} vs. particle size for the 5 different wavelengths of X-rays. Knowing the fact that the exact diameter for the nanocrystalline is 48.75 Å, these results show exact particle sizes. As the wavelength decreases, the energy of the wave

increases. The lower the wavelength, the higher the energy and momentum transfer vector. Q ≈ 60 $Å^{-1}$ for λ=0.21 Å and that yields relatively a high energy in comparison with the other wavelengths in this study. The result of this part is; The higher the energy of the wave, the closer the refined parameters to their expected values, but Q_{damp} is also an important parameter and must be refined as above. Figure 26 to Figure 40 also illustrate that besides the residual, other parameters must be checked in order to observe the quality and reliability of the fit. Nanocrystalline size, residual, lattice parameter, and ADP compared have proved to be exact when comparing with their real values [95].

CHAPTER III

CONCLUSION

X-ray diffraction and PDF analysis of nanocrystals was the focus of this research. Different ideal and energy-minimized conditions with different particle sizes and wavelengths have been considered and compared, to investigate the performance of the PDF analysis method under each circumstance, and as a function of each of these conditions. To observe the PDF of nanocrystals, two steps are required; 1) Simulating powder X-ray diffraction using Debye scattering equation on the nanocrystals 2) Fourier transforming the diffraction data into PDF data. PDF can also be obtained directly from the real space calculations of the materials, but it needs real space and number densities of the material, which might not be easy to obtain in case of unknown materials.

Energy-minimized nanocrystals were provided from LAMMPS [96], [97] and used in Debyer , PDFgetX3, and Diffpy-CMI. The pressure was kept constant at 10^5 pascals for all energy-minimized samples. Ideal nanocrystals were created by the VESTA software. All the samples were gold nanocrystals. Gold is a noble metal, meaning it resists chemical reactions and is highly suitable for in-situ studies [98]–[101]. The shape of all nanocrystals was spherical.

Different observations and comparisons have proven that nanocrystals' properties are different than the bulk counterparts. Smaller nanocrystals have drastic changes of behavior compared to their bulk samples [102]. Ideal nanocrystals have less diverged properties in comparison with energy-minimized nanocrystals.

X-ray diffraction patterns of all the samples are depicted in the results part. For the wavelength (λ) of 0.71073 Å, the end of the range (2θ =180°), a peak is detected which leads to higher uncertainties in the PDF pattern. As a result, the position of the cut should always be checked with Bragg's law to prevent unwanted high amounts of uncertainty in the resulting PDF analyses. For higher wavelengths, 0^{th} order peaks should be handled with care. In lower wavelengths, the peaks are thinner and have a lower FWHM. Intensity of the peaks is not a function of wavelength. In fact, Intensities are dependent on the number of electrons of the materials. Scattering factor refers to the same concept. As particle size increases, the intensities of the peaks increase. As wavelength increases, the peaks shift to the right-side of the graph.

Different refined parameters have been observed in this research. Parameters like particle size, lattice parameter and ADP show a considerable divergence of nanocrystal properties from the bulk materials. Particle size, based on real space calculations were compared with the particle size of PDF. Refined Particle sizes of PDF were close to the mean of the real space calculated diameters for all particle sizes. In PDF refinements, as the wavelength increased, the sizes increased for energy-minimized nanocrystals. However, there was no impact on the ideal particle size.

Q_{damp} was tested for a range of 0.001 to 0.02. This damping factor has a direct and powerful impact on all the refined parameters except lattice parameter. As a result, a safe range for Q_{damp} is the range that leads to a residual change of less than %1. That is why Q_{damp} was taken from 0.001 to 0.003. This range is safe and does not impact the refined results. The safest Q_{damp} values are the minimum amounts. The minimum possible Q_{damp} yields the minimum possible residual and most precise refined parameters.

PDF can also be for samples of various temperatures. As the temperature increases in a sample, the width of the PDF peaks increases, and their intensities decrease. The same happens to the diffraction peaks. Fitting a line to this pattern needs extra knowledge of Density Functional Theory and parameters like δ_1, δ_2 and Q_{broad}. The temperature-treated PDF fitting is the future work in this research.

APPENDIX A

Example command in PDFgetX3

$pdfgetx3 --verbose=info -t gr INPUTFILENAME -o OUTPUTFILENAME -w1.5418 --composition=Au --rmax=60 --qmin=1.7 --force=yes

The first comment calls the software “pdfgetx3”, “verbose” is the verbosity of the software, because the software has not a graphical interface, we need the verbosity command to see what the software is doing at each second and where the probable problems might happen, besides, the runtime and steps of the calculation are shown by verbosity. “t” shows the output file type. Instead of “INPUTFILENAME” and “OUTPUTFILENAME”, we are going to write the input and output file names. “W” stands for the wavelength of the illuminating X-ray and “composition” must be determined and defined for the software. The composition which was used in this research is Gold (Au). “rmax” is the maximum amount of “r” range and “qmin” is the minimum amount of “q” in the Fourier transformation or G(r). “force” means if there is already an output file with the same name, replace the current output file with the already existing file.

APPENDIX B

Example command in Diffpy-CMI

```
%matplotlib notebook
from matplotlib.pyplot import *
import string
from collections import OrderedDict
import numpy as np
from pyobjcryst import loadCrystal
from diffpy.srfit.pdf import DebyePDFGenerator, PDFGenerator, PDFParser
from diffpy.srfit.fitbase import Profile
from diffpy.srfit.fitbase import FitContribution, FitRecipe
from diffpy.srfit.fitbase import FitResults, initializeRecipe
from diffpy.Structure import Structure
from diffpy.Structure import loadStructure
from matplotlib import rcParams
# rcParams.update({'figure.autolayout': True})
# import matplotlib.pyplot as plt
import matplotlib.pyplot as plt
# plt.rcParams["figure.figsize"] = (6,6)



# Define functions for optimization and plotting that we will use later
```

```
def scipyOptimize(recipe):
    from scipy.optimize.minpack import leastsq
    print("Fit using scipy's LM optimizer")
    leastsq(recipe.residual, recipe.getValues())
    return


def plotRecipe(recipe, ax=None):
    """Plot recipe in the specified axes `ax`.

    If `ax` is None, create a new figure.

    Return `ax`
    """
#     if ax is None:
#         fig, ax = subplots()
    r = recipe.pdf.profile.x
    g = recipe.pdf.profile.y
    gcalc = recipe.pdf.evaluate()
    diffzero = -0.8 * max(g) * np.ones_like(g)
    diff = g - gcalc + diffzero
    plt.plot(r,g,'o',label="G(r) Data", mfc='none', mec='blue')
    plt.plot(r, gcalc,'r-',label="G(r) Fit")
    plt.plot(r,diff,'g-',label="G(r) diff")
    plt.plot(r, diffzero,'k-')
#    ax.set_title("$b)\lambda=0.560871\ \AA$")
#    ax.set_title("5nm_minimized($\lambda=0.560871\ \AA$)")
```

```
    plt.xlabel("$r (\AA)$")
    plt.ylabel("$G (\AA^{-2})$")
    plt.legend(loc=1)
    return plt

# Import the data and make it a PDFprofile.

grdata =  '*INPUTFILE*'
pdfprofile = Profile()
pdfparser = PDFParser()
pdfparser.parseFile(grdata)
pdfprofile.loadParsedData(pdfparser)

# Setup the PDFgenerator 1 that calculates the PDF from the CIF-file

pdfgenerator_crystal = PDFGenerator("G1")
pdfgenerator_crystal.setQmax(12.56)
pdfgenerator_crystal.setQmin(1.64)

# set qdamp, qbroad for the instrument
qdamp = 0.001
qbroad = 0.00
# Add the instrumental parameters to the two generators
pdfgenerator_crystal.qdamp.value = qdamp
pdfgenerator_crystal.qbroad.value = qbroad
```

```
# Load structure from the CIF file.

ciffile = "CIF File"
crystal_structure = loadCrystal(ciffile)
pdfgenerator_crystal.setStructure(crystal_structure)

# Add the profile and generator to the PDFcontribution
pdfcontribution = FitContribution("pdf")
pdfcontribution.setProfile(pdfprofile, xname="r")
pdfcontribution.addProfileGenerator(pdfgenerator_crystal)



# Setup correction scaling due to finite spherical shape. SP diameter from
PDFgui

from diffpy.srfit.pdf.characteristicfunctions import sphericalCF

pdfcontribution.registerFunction(sphericalCF, name="f1", argnames=['r',
'psize1'])

pdfcontribution.psize1 << 90;  # operator overloading- have different
meaning than default operators in python.

# Use scaling factors proportional to molar content
pdfcontribution.setEquation('mc1*G1*f1')
```

```
# Define the recipe to do the fit and add it to the PDFcontribution
recipe = FitRecipe()
recipe.addContribution(pdfcontribution)
# Avoid too much output during fitting
recipe.clearFitHooks()

# Add scale factor.
recipe.addVar(pdfcontribution.mc1, 1.0, tag = "scale")



#Add the delta2 parameters for the phase
recipe.addVar(pdfgenerator_crystal.delta2, 7, name = "delta2_crystal",
fixed=True, tag = "delta2")

# Add the psize variable for diameter of the spherical nanoparticle.
recipe.addVar(pdfcontribution.psize1);

# Add the structural paramters using space group constaints for the crystal
phase_crystal = pdfgenerator_crystal.phase
sgpars_crystal = phase_crystal.sgpars

for par in sgpars_crystal.latpars:
    recipe.addVar(par, name=par.name+'_s', tag='cell')

# assign isotropic ADP
```

```
recipe.newVar(name='Biso_Au', value=0.001,fixed=True,tag="ADP_atom")


scatterers=phase_crystal.getScatterers()


for s in scatterers:
    recipe.constrain(s.Biso,"Biso_Au")




# Set the r-range to fit
pdfprofile.setCalculationRange(xmin = 2, xmax = 60, dx=0.01)


# First refine only the scale
recipe.fix('all') # Fix the parameters written in the bracket, in this case all of them
recipe.free('scale', 'cell') #Free the parameters with the tag 'scale' and 'xyz'
scipyOptimize(recipe) # Do the least-square refinement
# recipe.free('ADP_atom') #Free the parameters with the tag 'adp_zr'
# scipyOptimize(recipe) # Do the least-square refinement
#recipe.free('delta2_crystal') ##Free the parameter delta2_crystal
#scipyOptimize(recipe) # Do the least-square refinement again with the extra freed parameter


recipe.free('psize1') ##Free the parameter psize1
scipyOptimize(recipe) # Do the least-square refinement again with the extra freed parameter
```

```
recipe.free('ADP_atom')
scipyOptimize(recipe)

print(FitResults(recipe)) # Print the results from the fit
plotRecipe(recipe); # Plot the fit

plt.show()
```

APPENDIX C

Allowed reflections for cubic unit cells

Table 14 Allowed reflections from Simple Cubic (SC), Base Centered Cubic (BCC), and Face Centered Cubic (FCC) unit cells.

h	*k*	*l*	$h^2+k^2+l^2$	*SC*	*BCC*	*FCC*
1	0	0	1	✓		
1	1	0	2	✓	✓	
1	1	1	3	✓		✓
2	0	0	4	✓	✓	✓
2	1	0	5	✓		
2	1	1	6	✓	✓	
2	2	0	8	✓	✓	✓
2	2	1	9	✓		
2	2	2	12	✓	✓	✓
3	0	0	9	✓		
3	1	0	10	✓	✓	
3	1	1	11	✓		✓
3	2	0	13	✓		
3	2	1	14	✓	✓	
3	2	2	17	✓		
3	3	0	18	✓	✓	
3	3	1	19	✓		✓
3	3	2	22	✓	✓	
3	3	3	27	✓		✓
4	0	0	16	✓	✓	✓
4	1	0	17	✓		
4	1	1	18	✓	✓	
4	2	0	20	✓	✓	✓
4	2	1	21	✓		
4	2	2	24	✓	✓	✓
4	3	0	25	✓		
4	3	1	26	✓	✓	
4	3	2	29	✓		
4	3	3	34	✓	✓	

APPENDIX D

Shape factors

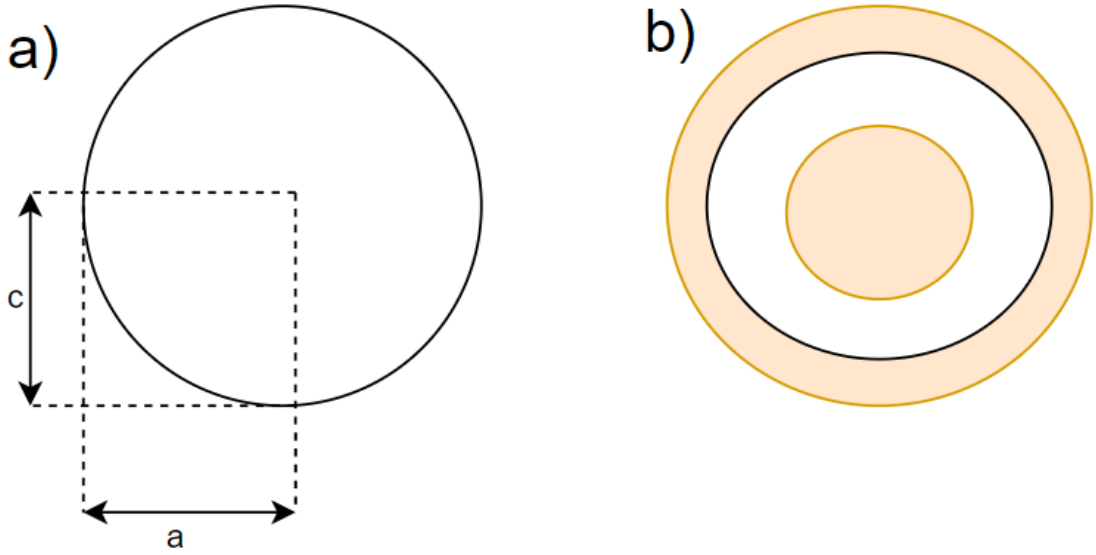

Figure 42 a) prolate and oblate ellipsoids. **b)** core and shell spheroids.

If a and c are equal, the ellipsoid is a spheroid. There is going to be two scenarios for a and c:

1. $e = (1 - \frac{a^2}{c^2})^{\frac{1}{2}}$, for prolate spheroids (c>a)

2. $e = (1 - \frac{c^2}{a^2})^{\frac{1}{2}}$, for oblate spheroids (c<a)

Based on the above figure and relation of c/a, the ellipsoid can be considered as prolate or oblate. Core and shell spheroids consist of a core of atoms in the middle of the system and a shell which has little or no contact with the core.

Considering spheroids, the shape function can be obtained from:

$$f_{spheroid}(r) = \int_{\theta_{min}}^{\theta_{max}} f_{sphere}\,(r', D).\, sin\theta\,.\, d\theta\,, D = 2r$$

$$\boldsymbol{r'(\theta) = rR\left(\frac{sin^2\theta}{a^2} + \frac{cos^2\theta}{c^2}\right)^{\frac{1}{2}}}$$

$$\boldsymbol{\eta = \sqrt{1 - e^2}}$$

The Shape functions can be derived using the above equations. Spherical shape functions are as below [51]:

$$f_{sphere}(r, D) = 1 - \frac{3}{2}\left(\frac{r}{D}\right) + \frac{1}{2}\left(\frac{r}{D}\right)^3$$

where “r” is the atomic pair distance, and “D” is the diameter of the spherical nanocrystalline.

BIBLIOGRAPHY

[1] S. Xiong, H. Öztürk, S. Y. Lee, P. M. Mooney, and I. C. Noyan, "The nanodiffraction problem," *J. Appl. Crystallogr.*, vol. 51, no. 4, 2018, doi: 10.1107/S1600576718007719.

[2] T. Egami and S. J. L. Billinge, "Underneath the Bragg Peaks," *Mater. Today*, vol. 6, no. 6, 2003, doi: 10.1016/s1369-7021(03)00635-7.

[3] H. S. Geddes, H. Blade, J. F. McCabe, L. P. Hughes, and A. L. Goodwin, "Structural characterisation of amorphous solid dispersions: Via metropolis matrix factorisation of pair distribution function data," *Chem. Commun.*, vol. 55, no. 89, 2019, doi: 10.1039/c9cc06753a.

[4] T. Proffen, S. J. L. Billinge, T. Egami, and D. Louca, "Structural analysis of complex materials using the atomic pair distribution function - A practical guide," *Zeitschrift fur Kristallographie*, vol. 218, no. 2. 2003, doi: 10.1524/zkri.218.2.132.20664.

[5] H. Van Swygenhoven, M. Spaczer, and A. Caro, "Role of low and high angle grain boundaries in the deformation mechanism of nanophase Ni: A molecular dynamics simulation study," *Nanostructured Mater.*, vol. 10, no. 5, 1998, doi: 10.1016/S0965-9773(98)00118-4.

[6] P. M. Derlet and H. Van Swygenhoven, "Atomic positional disorder in fcc metal nanocrystalline grain boundaries," *Phys. Rev. B - Condens. Matter Mater. Phys.*, vol. 67, no. 1, 2003, doi: 10.1103/PhysRevB.67.014202.

[7] H. P. Wang, C. H. Zheng, P. F. Zou, S. J. Yang, L. Hu, and B. Wei, "Density determination and simulation of Inconel 718 alloy at normal and metastable liquid states," *J. Mater. Sci. Technol.*, vol. 34, no. 3, 2018, doi: 10.1016/j.jmst.2017.10.014.

[8] R. F. Mould, "Röntgen and the discovery of X-rays," *Br. J. Radiol.*, vol. 68, no. 815, 1995, doi: 10.1259/0007-1285-68-815-1145.

[9] S. Zabler, P. Cloetens, J. P. Guigay, J. Baruchel, and M. Schlenker, "Optimization of phase contrast imaging using hard x rays," *Rev. Sci. Instrum.*, vol. 76, no. 7, 2005, doi: 10.1063/1.1960797.

[10] S. Banerjee *et al.*, "Cluster-mining: An approach for determining core structures of metallic nanoparticles from atomic pair distribution function data Banerjee Soham," *Acta Crystallogr. Sect. A Found. Adv.*, vol. 76, 2020, doi: 10.1107/S2053273319013214.

[11] M. Eckert, "Max von Laue and the discovery of X-ray diffraction in 1912," *Annalen der Physik*, vol. 524, no. 5. 2012, doi: 10.1002/andp.201200724.

[12] A. Brown and H. Suit, "The centenary of the discovery of the Bragg peak," *Radiother. Oncol.*, vol. 73, no. 3, 2004, doi: 10.1016/j.radonc.2004.09.008.

[13] F. Lauraux *et al.*, "Simultaneous multi-bragg peak coherent X-ray diffraction imaging," *Crystals*, vol. 11, no. 3, 2021, doi: 10.3390/cryst11030312.

[14] C. G. Pope, “X-ray diffraction and the bragg equation,” *J. Chem. Educ.*, vol. 74, no. 1, 1997, doi: 10.1021/ed074p129.

[15] Y. Jiang, L. Cao, X. Hu, Z. Ren, C. Zhang, and C. Wang, “Simulating Powder X-ray Diffraction Patterns of Two-Dimensional Materials,” *Inorg. Chem.*, vol. 57, no. 24, 2018, doi: 10.1021/acs.inorgchem.8b02315.

[16] P. Debye, “Zerstreuung von Röntgenstrahlen,” *Ann. Phys.*, vol. 351, no. 6, 1915, doi: 10.1002/andp.19153510606.

[17] M. Sestu, A. Corrias, M. Casula, and G. Navarra, “Debye function and Reverse Monte Carlo refinement of nano-sized FeOOH,” *Acta Crystallogr. Sect. A Found. Adv.*, vol. 70, no. a1, 2014, doi: 10.1107/s2053273314085544.

[18] P. Scardi, S. J. L. Billinge, R. Neder, and A. Cervellino, “Celebrating 100 years of the Debye scattering equation,” *Acta Crystallographica Section A: Foundations and Advances*, vol. 72, no. 6. 2016, doi: 10.1107/S2053273316015680.

[19] “COMPUTATIONAL ANALYSIS OF DIFFRACTION IN IDEAL NANOCRYSTALLINE POWDERS ¨Hande Ozturk¨,” *PhD Diss.*, 2015.

[20] V. I. Punegov, S. I. Kolosov, and K. M. Pavlov, “Bragg-Laue X-ray dynamical diffraction on perfect and deformed lateral crystalline structures,” *J. Appl. Crystallogr.*, vol. 49, no. 4, 2016, doi: 10.1107/S1600576716008396.

[21] S. Billinge, “The nanostructure problem,” *Physics (College. Park. Md).*, vol. 3, 2010, doi: 10.1103/physics.3.25.

[22] E. E. Fullerton, I. K. Schuller, H. Vanderstraeten, and Y. Bruynseraede, “Structural refinement of superlattices from x-ray diffraction,” *Phys. Rev. B*, vol. 45, no. 16, 1992, doi: 10.1103/PhysRevB.45.9292.

[23] Y. Waseda, E. Matsubara, and K. Shinoda, *X-Ray Diffraction Crystallography; Introduction, examples and solved problems*. 2011.

[24] K. Zhang, I. V. Alexandrov, R. Z. Valiev, and K. Lu, “Structural characterization of nanocrystalline copper by means of x-ray diffraction,” *Journal of Applied Physics*, vol. 80, no. 10. 1996, doi: 10.1063/1.363612.

[25] Y. Bouhadda, D. Bormann, E. Sheu, D. Bendedouch, A. Krallafa, and M. Daaou, “Characterization of Algerian Hassi-Messaoud asphaltene structure using Raman spectrometry and X-ray diffraction,” *Fuel*, vol. 86, no. 12–13, 2007, doi: 10.1016/j.fuel.2006.12.006.

[26] F. T. L. Muniz, M. A. R. Miranda, C. Morilla Dos Santos, and J. M. Sasaki, “The Scherrer equation and the dynamical theory of X-ray diffraction,” *Acta Crystallogr. Sect. A Found. Adv.*, vol. 72, no. 3, 2016, doi: 10.1107/S205327331600365X.

[27] J. I. Langford and A. J. C. Wilson, “Scherrer after sixty years: A survey and some new results in the determination of crystallite size,” *J. Appl. Crystallogr.*, vol. 11, no. 2, 1978, doi: 10.1107/s0021889878012844.

[28] A. Khorsand Zak, W. H. Abd. Majid, M. E. Abrishami, and R. Yousefi, “X-ray analysis of ZnO nanoparticles by Williamson-Hall and size-strain plot methods,” *Solid State Sci.*, vol. 13, no. 1, 2011, doi: 10.1016/j.solidstatesciences.2010.11.024.

[29] Y. Iwasa *et al.*, “New phases of C60 synthesized at high pressure,” *Science (80-.).*, vol. 264, no. 5165, 1994, doi: 10.1126/science.264.5165.1570.

[30] R. Yogamalar, R. Srinivasan, A. Vinu, K. Ariga, and A. C. Bose, “X-ray peak broadening analysis in ZnO nanoparticles,” *Solid State Commun.*, vol. 149, no. 43–44, 2009, doi: 10.1016/j.ssc.2009.07.043.

[31] S. J. L. Billinge and I. Levin, “The problem with determining atomic structure at the nanoscale,” *Science*, vol. 316, no. 5824. 2007, doi: 10.1126/science.1135080.

[32] P. Mao, “Photo by Piseth Mao from Pexels.” https://www.pexels.com/photo/a-5x5-rubik-cube-puzzle-on-white-table-5509887/.

[33] J. Thomas, “Photo by Jadson Thomas from Pexels.” https://www.pexels.com/photo/3-by-3-rubik-s-cube-selective-focus-photography-1500610/.

[34] X. S. Yan, P. Lin, X. Qi, and L. Yang, “Finnis-Sinclair potentials for fcc Au-Pd and Ag-Pt alloys,” *Int. J. Mater. Res.*, vol. 102, pp. 381–388, 2011.

[35] I. K. Suh, H. Ohta, and Y. Waseda, “High-temperature expansion of six metallic elements measured by dilatation method and X-ray diffraction,” *J. Mater. Sci.*, vol. 23, pp. 757–760, 1988.

[36] J. J. Couderc, G. Garigue, L. Lafourcade, and Q. T. Nguyen, “Eine Versuchsanordnung und Beispiele zur kontinuierlichen Strukturanalyse mit Roentgenstahlen,” *Zeitschrift fuer Met.*, vol. 50, pp. 708–716, 1959.

[37] M. W. Heaven, A. Dass, P. S. White, K. M. Holt, and R. W. Murray, “Crystal structure of the gold nanoparticle [N(C8H 17)4][Au25(SCH2CH 2Ph)18],” *J. Am. Chem. Soc.*, vol. 130, no. 12, 2008, doi: 10.1021/ja800561b.

[38] A. Bayler, A. Schier, G. A. Bowmaker, and H. Schmidbaur, “Gold is smaller than silver. Crystal structures of [bis(trimesitylphosphine)gold(I)] and [bis(trimesitylphosphine)silver(I)] tetrafluoroborate,” *J. Am. Chem. Soc.*, vol. 118, no. 29, 1996, doi: 10.1021/ja961363v.

[39] D. Prill, P. Juhás, S. J. L. Billinge, and M. U. Schmidt, “Towards solution and refinement of organic crystal structures by fitting to the atomic pair distribution function,” *Acta Crystallogr. Sect. A Found. Adv.*, vol. 72, 2016, doi: 10.1107/S2053273315022457.

[40] D. Errandonea, D. Santamaria-Perez, V. Grover, S. N. Achary, and A. K. Tyagi, “High-pressure x-ray diffraction study of bulk and nanocrystalline PbMoO4,” *J. Appl. Phys.*, vol. 108, no. 7, 2010, doi: 10.1063/1.3493048.

[41] P. Dutta, M. S. Seehra, S. Thota, and J. Kumar, “A comparative study of the magnetic properties of bulk and nanocrystalline Co3O4,” *J. Phys. Condens. Matter*, vol. 20, no. 1, 2008, doi: 10.1088/0953-8984/20/01/015218.

[42] B. N. Dutta and B. Dayal, “Lattice constants and thermal expansion of gold up to 878 C by X-ray method,” *Phys. Status Solidi*, vol. 3, pp. 473–477, 1963.

[43] R. C. Agarwal, “A new least-squares refinement technique based on the fast Fourier transform algorithm,” *Acta Crystallogr. Sect. A*, vol. 34, no. 5, 1978, doi: 10.1107/S0567739478001618.

[44] J. P. Dismukes, L. Ekstrom, and R. J. Paff, “Lattice parameter and density in germanium-silicon alloys,” *J. Phys. Chem.*, vol. 68, no. 10, 1964, doi: 10.1021/j100792a049.

[45] P. F. Peterson, E. S. Božin, T. Proffen, and S. J. L. Billinge, “Improved measures of

quality for the atomic pair distribution function," *J. Appl. Crystallogr.*, vol. 36, no. 1, 2003, doi: 10.1107/S0021889802018708.

[46] A. P. Dudka, N. B. Bolotina, and O. N. Khrykina, "DebyeFit: a simple tool to obtain an appropriate model of atomic vibrations in solids from atomic displacement parameters obtained at different temperatures," *J. Appl. Crystallogr.*, vol. 52, no. 3, 2019, doi: 10.1107/S1600576719005818.

[47] M. H. Braga, J. J. A. Ferreira, J. Siewenie, T. Proffen, S. C. Vogel, and L. L. Daemen, "Neutron powder diffraction and first-principles computational studies of CuLixMg2-x (x≅0.08), CuMg2, and Cu2Mg," *J. Solid State Chem.*, vol. 183, no. 1, 2010, doi: 10.1016/j.jssc.2009.09.010.

[48] A. S. Masadeh *et al.*, "Quantitative size-dependent structure and strain determination of CdSe nanoparticles using atomic pair distribution function analysis," *Phys. Rev. B - Condens. Matter Mater. Phys.*, vol. 76, no. 11, 2007, doi: 10.1103/PhysRevB.76.115413.

[49] T. K. Boehme and R. Bracewell, "The Fourier Transform and its Applications.," *Am. Math. Mon.*, vol. 73, no. 6, 1966, doi: 10.2307/2314845.

[50] T. Dykhne, R. Taylor, A. Florence, and S. J. L. Billinge, "Data requirements for the reliable use of atomic pair distribution functions in amorphous pharmaceutical fingerprinting," *Pharm. Res.*, vol. 28, no. 5, 2011, doi: 10.1007/s11095-010-0350-0.

[51] B. Gilbert, "Finite size effects on the real-space pair distribution function of nanoparticles," *J. Appl. Crystallogr.*, vol. 41, no. 3, pp. 554–562, 2008, doi: 10.1107/S0021889808007905.

[52] R. B. Neder and V. I. Korsunskiy, "Structure of nanoparticles from powder diffraction data using the pair distribution function," in *Journal of Physics Condensed Matter*, 2005, vol. 17, no. 5 SPEC. ISS., doi: 10.1088/0953-8984/17/5/013.

[53] T. D. Davis, "Fingerprinting analysis of non-crystalline pharmaceutical compounds using high energy X-rays and the total scattering pair distribution function," p. 215, 2011.

[54] V. Petkov, "Pair Distribution Functions Analysis," *Charact. Mater.*, pp. 1361–1372, 2012, doi: 10.1002/0471266965.com159.

[55] D. Olds, C. N. Saunders, M. Peters, T. Proffen, J. Neuefeind, and K. Page, "Precise implications for real-space pair distribution function modeling of effects intrinsic to modern time-of-flight neutron diffractometers," *Acta Crystallogr. Sect. A Found. Adv.*, vol. 74, no. 4, 2018, doi: 10.1107/S2053273318003224.

[56] T. L. Christiansen, S. R. Cooper, and K. M. O. Jensen, "There's no place like real-space: Elucidating size-dependent atomic structure of nanomaterials using pair distribution function analysis," *Nanoscale Adv.*, vol. 2, no. 6, 2020, doi: 10.1039/d0na00120a.

[57] S. J. L. Billinge, "The rise of the X-ray atomic pair distribution function method: a series of fortunate events," *Philos. Trans. R. Soc. A Math. Phys. Eng. Sci.*, vol. 377, no. 2147, 2019, doi: 10.1098/rsta.2018.0413.

[58] C. D. Martin, S. M. Antao, P. J. Chupas, P. L. Lee, S. D. Shastri, and J. B. Parise, "Quantitative high-pressure pair distribution function analysis of nanocrystalline gold," *Appl. Phys. Lett.*, vol. 86, no. 6, pp. 1–3, Feb. 2005, doi: 10.1063/1.1856691.

[59] C. L. Farrow and S. J. L. Billinge, "Relationship between the atomic pair distribution function and small-angle scattering: Implications for modeling of nanoparticles," *Acta*

Crystallogr. Sect. A Found. Crystallogr., vol. 65, no. 3, 2009, doi: 10.1107/S0108767309009714.

[60] C. N. Singman, "Atomic volume and allotropy of the elements," *J. Chem. Educ.*, vol. 61, no. 2, 1984, doi: 10.1021/ed061p137.

[61] C. L. Farrow *et al.*, "PDFfit2 and PDFgui: Computer programs for studying nanostructure in crystals," *J. Phys. Condens. Matter*, vol. 19, no. 33, Aug. 2007, doi: 10.1088/0953-8984/19/33/335219.

[62] B. Gilbert, F. Huang, H. Zhang, G. A. Waychunas, and J. F. Banfield, "Nanoparticles: Strained and stiff," *Science (80-.).*, vol. 305, no. 5684, 2004, doi: 10.1126/science.1098454.

[63] K. Kodama, S. Iikubo, T. Taguchi, and S. I. Shamoto, "Finite size effects of nanoparticles on the atomic pair distribution functions," *Acta Crystallogr. Sect. A Found. Crystallogr.*, vol. 62, no. 6, pp. 444–453, 2006, doi: 10.1107/S0108767306034635.

[64] S. J. L. Billinge, "Diffpy Google Forum," [Online]. Available: diffpy-users@googlegroups.com.

[65] M. W. Terban and S. J. L. Billinge, "Structural Analysis of Molecular Materials Using the Pair Distribution Function," *Chem. Rev.*, 2021, doi: 10.1021/acs.chemrev.1c00237.

[66] X. Wang, B. Jiang, and J. S. Liu, "Generalized R-squared for detecting dependence," *Biometrika*, vol. 104, no. 1, 2017, doi: 10.1093/biomet/asw071.

[67] A. C. Cameron and F. A. G. Windmeijer, "An R-squared measure of goodness of fit for some common nonlinear regression models," *J. Econom.*, vol. 77, no. 2, 1997, doi: 10.1016/s0304-4076(96)01818-0.

[68] J. D. Rights and S. K. Sterba, "Quantifying explained variance in multilevel models: An integrative framework for defining R-squared measures," *Psychol. Methods*, vol. 24, no. 3, 2019, doi: 10.1037/met0000184.

[69] S. Wu, "3 Best metrics to evaluate Regression Model?," [Online]. Available: https://towardsdatascience.com/what-are-the-best-metrics-to-evaluate-your-regression-model-418ca481755b.

[70] M. Wojdyr, "Debyer Software Package." https://github.com/wojdyr/debyer.

[71] S. J. L. Billinge, "PDFgetX3," [Online]. Available: https://www.diffpy.org/doc/pdfgetx3/tutorial.html.

[72] S. J. L. Billinge, "Diffpy-CMI," [Online]. Available: https://www.diffpy.org/products/diffpycmi/index.html.

[73] L. Gamez-Mendoza, M. W. Terban, S. J. L. Billinge, and M. Martinez-Inesta, "Modelling and validation of particle size distributions of supported nanoparticles using the pair distribution function technique," *J. Appl. Crystallogr.*, vol. 50, no. 3, 2017, doi: 10.1107/S1600576717003715.

[74] P. J. Chupas, K. W. Chapman, and P. L. Lee, "Applications of an amorphous silicon-based area detector for high-resolution, high-sensitivity and fast time-resolved pair distribution function measurements," *J. Appl. Crystallogr.*, vol. 40, no. 3, 2007, doi: 10.1107/S0021889807007856.

[75] A. Kovyahk, "X-ray pair distribution function analysis of transition and noble metals for

industrial applications in sensing and catalysis," 2018.

[76] I. K. Jeong, T. Proffen, F. Mohiuddin-Jacobs, and S. J. L. Billinge, "Measuring Correlated Atomic Motion Using X-ray Diffraction," *J. Phys. Chem. A*, vol. 103, no. 7, 1999, doi: 10.1021/jp9836978.

[77] M. Billinge, Simon, Juhas, Pavol, Farrow, Christopher, and McKerns, "DiffPy-CMI-Python libraries for Complex Modeling Initiative.," *Web.*, vol. Vers. 00., [Online]. Available: https://www.osti.gov//servlets/purl/1231727.

[78] P. Juhás and S. J. L. Billinge, " DiffPy-CMI – a software toolbox for structure analysis by complex modeling method ," *Acta Crystallogr. Sect. A Found. Adv.*, vol. 73, no. a1, 2017, doi: 10.1107/s0108767317096210.

[79] B. A. Frandsen *et al.*, "Local atomic and magnetic structure of dilute magnetic semiconductor (Ba, K)(Zn,Mn)2As2," *Phys. Rev. B*, vol. 94, no. 9, 2016, doi: 10.1103/PhysRevB.94.094102.

[80] R. B. Neder and T. Proffen, "Exact and fast calculation of the X-ray pair distribution function," *J. Appl. Crystallogr.*, vol. 53, 2020, doi: 10.1107/S1600576720004616.

[81] X. Yang, A. S. Masadeh, J. R. McBride, E. S. Božin, S. J. Rosenthal, and S. J. L. Billinge, "Confirmation of disordered structure of ultrasmall CdSe nanoparticles from X-ray atomic pair distribution function analysis," *Phys. Chem. Chem. Phys.*, vol. 15, no. 22, 2013, doi: 10.1039/c3cp00111c.

[82] J. Quinson, L. Kacenauskaite, T. L. Christiansen, T. Vosch, M. Arenz, and K. M. Ø. Jensen, "Spatially Localized Synthesis and Structural Characterization of Platinum Nanocrystals Obtained Using UV Light," *ACS Omega*, vol. 3, no. 8, 2018, doi: 10.1021/acsomega.8b01613.

[83] S. L. J. Thomae, N. Prinz, T. Hartmann, M. Teck, S. Correll, and M. Zobel, "Pushing data quality for laboratory pair distribution function experiments," *Rev. Sci. Instrum.*, vol. 90, no. 4, 2019, doi: 10.1063/1.5093714.

[84] V. Petkov, "Nanostructure by high-energy X-ray diffraction," *Materials Today*, vol. 11, no. 11. 2008, doi: 10.1016/S1369-7021(08)70236-0.

[85] C. F. Holder and R. E. Schaak, "Tutorial on Powder X-ray Diffraction for Characterizing Nanoscale Materials," *ACS Nano*, vol. 13, no. 7. 2019, doi: 10.1021/acsnano.9b05157.

[86] W. Reimers *et al.*, "Evaluation of residual stresses in the bulk of materials by high energy synchrotron diffraction," *J. Nondestruct. Eval.*, vol. 17, no. 3, 1998, doi: 10.1023/A:1022607030355.

[87] W. Reimers *et al.*, "Use of high-energy synchrotron diffraction for residual stress analyses," *J. Mater. Sci. Lett.*, vol. 18, no. 7, 1999, doi: 10.1023/A:1006651217517.

[88] G. Leinders, T. Cardinaels, K. Binnemans, and M. Verwerft, "Accurate lattice parameter measurements of stoichiometric uranium dioxide," *J. Nucl. Mater.*, vol. 459, 2015, doi: 10.1016/j.jnucmat.2015.01.029.

[89] T. Wang, J. Zhu, R. A. Mackay, L. Q. Chen, and Z. K. Liu, "Modeling of lattice parameter in the Ni-Al system," *Metall. Mater. Trans. A Phys. Metall. Mater. Sci.*, vol. 35 A, no. 8, 2004, doi: 10.1007/s11661-006-0211-y.

[90] H. L. Kim, J. S. Park, and Y. W. Chang, "Effects of lattice parameter changes on critical resolved shear stress and mechanical properties of magnesium binary single crystals,"

Mater. Sci. Eng. A, vol. 540, 2012, doi: 10.1016/j.msea.2012.01.126.

[91] C. Burns, W. U. Spendel, S. Puckett, and G. E. Pacey, "Solution ionic strength effect on gold nanoparticle solution color transition," *Talanta*, vol. 69, no. 4, 2006, doi: 10.1016/j.talanta.2005.11.038.

[92] A. D. McFarland, C. L. Haynes, C. A. Mirkin, R. P. Van Duyne, and H. A. Godwin, "Color My Nanoworld," *J. Chem. Educ.*, vol. 81, no. 4, 2004, doi: 10.1021/ed081p544a.

[93] M. Iwaki, A. H. Iwane, K. Ikezaki, and T. Yanagida, "Local Heat Activation of Single Myosins Based on Optical Trapping of Gold Nanoparticles," *Nano Lett.*, vol. 15, no. 4, 2015, doi: 10.1021/nl5049059.

[94] R. G. Haverkamp and K. S. Wallwork, "X-ray pair distribution function analysis of nano-structured materials using a Mythen detector," *J. Synchrotron Radiat.*, vol. 16, no. 6, pp. 849–856, 2009, doi: 10.1107/S0909049509036723.

[95] H. Ö. Abolfazl Baloochiyan, Merdan Batyrov, "Accuracy limits of pair distribution function analysis in structural characterization of nanocrystalline powders by X-ray diffraction," doi: 10.3906/fiz-1.

[96] "LAMMPS website." https://www.lammps.org/index.html.

[97] A. P. Thompson *et al.*, "LAMMPS - a flexible simulation tool for particle-based materials modeling at the atomic, meso, and continuum scales," *Comput. Phys. Commun.*, vol. 271, 2022, doi: 10.1016/j.cpc.2021.108171.

[98] M. Teimouri *et al.*, "Gold nanoparticles fabrication by plant extracts: synthesis, characterization, degradation of 4-nitrophenol from industrial wastewater, and insecticidal activity – A review," *Journal of Cleaner Production*, vol. 184. 2018, doi: 10.1016/j.jclepro.2018.02.268.

[99] D. A. Giljohann, D. S. Seferos, W. L. Daniel, M. D. Massich, P. C. Patel, and C. A. Mirkin, "Gold nanoparticles for biology and medicine," *Angewandte Chemie - International Edition*, vol. 49, no. 19. 2010, doi: 10.1002/anie.200904359.

[100] M. Das, K. H. Shim, S. S. A. An, and D. K. Yi, "Review on gold nanoparticles and their applications," *Toxicology and Environmental Health Sciences*, vol. 3, no. 4. 2011, doi: 10.1007/s13530-011-0109-y.

[101] K. Sztandera, M. Gorzkiewicz, and B. Klajnert-Maculewicz, "Gold Nanoparticles in Cancer Treatment," *Molecular Pharmaceutics*, vol. 16, no. 1. 2019, doi: 10.1021/acs.molpharmaceut.8b00810.

[102] J. E. Jørgensen, J. M. Jakobsen, J. Z. Jiang, L. Gerward, and J. S. Olsen, "High-pressure X-ray diffraction study of bulk- and nanocrystalline GaN," *J. Appl. Crystallogr.*, vol. 36, no. 3 II, 2003, doi: 10.1107/S0021889803005375.

[103] M. Sakata and M. J. Cooper, "An analysis of the Rietveld refinement method," *J. Appl. Crystallogr.*, vol. 12, no. 6, 1979, doi: 10.1107/s002188987901325x.

[104] R. B. Von Dreele, "Quantitative texture analysis by Rietveld refinement," *J. Appl. Crystallogr.*, vol. 30, no. 4, 1997, doi: 10.1107/S0021889897005918.

VITA

EDUCATION

Master of Science student in Mechanical Engineering at **Özyeğin University**. *January 2020 – December 2021.* Thesis title: "Investigation of pair distribution function method on structural analysis of X-ray diffraction data from nanocrystalline powders."

Bachelor of Engineering Science, Mechanical Engineering at **University of Tehran**. *September 2014 - March 2019*.

ACADEMIC EMPLOYMENT

Graduate Teaching Assistant, department of Mechanical Engineering, **Özyeğin University.** *January 2020 – December 2021*.

PUBLICATIONS

Baloochiyan, Batyrov, Öztürk. "Accuracy limits of pair distribution function analysis in structural characterization of nanocrystalline powders by X-ray diffraction." (in review).